# Interannual and (multi-)decadal variability in the sedimentary BIT index of Lake Challa, East Africa, over the past 2200 years: assessment of the precipitation proxy

Buckles, L. K., Verschuren, D., Weijers, J. W. H., Cocquyt, C., Blaauw, M., & Damste, J. S. S. (2016). Interannual and (multi-)decadal variability in the sedimentary BIT index of Lake Challa, East Africa, over the past 2200 years: assessment of the precipitation proxy. *Climate of the Past*, *12*, 1243-1262. https://doi.org/10.5194/cp-12-1243-2016

**Published in:**
Climate of the Past

**Document Version:**
Publisher's PDF, also known as Version of record

Clim. Past, 12, 1243–1262, 2016
www.clim-past.net/12/1243/2016/
doi:10.5194/cp-12-1243-2016


Climate of the Past
Open Access
EGU

# Interannual and (multi-)decadal variability in the sedimentary BIT index of Lake Challa, East Africa, over the past 2200 years: assessment of the precipitation proxy

**Laura K. Buckles[1], Dirk Verschuren[2], Johan W. H. Weijers[1,a], Christine Cocquyt[3], Maarten Blaauw[4], and Jaap S. Sinninghe Damsté[1,5]**

[1]University of Utrecht, Faculty of Geosciences, P.O. Box 80.021, 3508 TA Utrecht, the Netherlands
[2]Limnology Unit, Department of Biology, Ghent University, K. L. Ledeganckstraat 35, 9000 Gent, Belgium
[3]Botanic Garden Meise, Nieuwelaan 38, 1860 Meise, Belgium
[4]School of Geography, Archaeology and Palaeoecology, Queen's University Belfast, Elmwood Avenue, Belfast BT7 1NN, UK
[5]NIOZ Royal Netherlands Institute for Sea Research, Department of Marine Microbiology and Biogeochemistry, and Utrecht University, P.O. Box 59, 1790 AB Den Burg, Texel, the Netherlands
[a]present address: Shell Global Solutions International B.V., Kessler Park 1, 2288 GS Rijswijk, the Netherlands

*Correspondence to:* Jaap S. Sinninghe Damsté (damste@nioz.nl)

Received: 9 February 2015 – Published in Clim. Past Discuss.: 2 April 2015
Revised: 28 April 2016 – Accepted: 13 May 2016 – Published: 27 May 2016

**Abstract.** The branched vs. isoprenoid tetraether (BIT) index is based on the relative abundance of branched tetraether lipids (brGDGTs) and the isoprenoidal GDGT crenarchaeol. In Lake Challa sediments the BIT index has been applied as a proxy for local monsoon precipitation on the assumption that the primary source of brGDGTs is soil washed in from the lake's catchment. Since then, microbial production within the water column has been identified as the primary source of brGDGTs in Lake Challa sediments, meaning that either an alternative mechanism links BIT index variation with rainfall or that the proxy's application must be reconsidered. We investigated GDGT concentrations and BIT index variation in Lake Challa sediments at a decadal resolution over the past 2200 years, in combination with GDGT time-series data from 45 monthly sediment-trap samples and a chronosequence of profundal surface sediments.

Our 2200-year geochemical record reveals high-frequency variability in GDGT concentrations, and therefore in the BIT index, superimposed on distinct lower-frequency fluctuations at multi-decadal to century timescales. These changes in BIT index are correlated with changes in the concentration of crenarchaeol but not with those of the brGDGTs. A clue for understanding the indirect link between rainfall and crenarchaeol concentration (and thus thaumarchaeotal abundance) was provided by the observation that surface sediments collected in January 2010 show a distinct shift in GDGT composition relative to sediments collected in August 2007. This shift is associated with increased bulk flux of settling mineral particles with high Ti / Al ratios during March–April 2008, reflecting an event of unusually high detrital input to Lake Challa concurrent with intense precipitation at the onset of the principal rain season that year. Although brGDGT distributions in the settling material are initially unaffected, this soil-erosion event is succeeded by a massive dry-season diatom bloom in July–September 2008 and a concurrent increase in the flux of GDGT-0. Complete absence of crenarchaeol in settling particles during the austral summer following this bloom indicates that no Thaumarchaeota bloom developed at that time. We suggest that increased nutrient availability, derived from the eroded soil washed into the lake, caused the massive bloom of diatoms and that the higher concentrations of ammonium (formed from breakdown of this algal matter) resulted in a replacement of nitrifying Thaumarchaeota, which in typical years prosper during the austral summer, by nitrifying bacteria. The decomposing dead diatoms passing through the suboxic zone of the water column

probably also formed a substrate for GDGT-0-producing archaea. Hence, through a cascade of events, intensive rainfall affects thaumarchaeotal abundance, resulting in high BIT index values.

Decade-scale BIT index fluctuations in Lake Challa sediments exactly match the timing of three known episodes of prolonged regional drought within the past 250 years. Additionally, the principal trends of inferred rainfall variability over the past two millennia are consistent with the hydroclimatic history of equatorial East Africa, as has been documented from other (but less well dated) regional lake records. We therefore propose that variation in GDGT production originating from the episodic recurrence of strong soil-erosion events, when integrated over (multi-)decadal and longer timescales, generates a stable positive relationship between the sedimentary BIT index and monsoon rainfall at Lake Challa. Application of this paleoprecipitation proxy at other sites requires ascertaining the local processes which affect the productivity of crenarchaeol by Thaumarchaeota and brGDGTs.

## 1 Introduction

Geographically widespread isoprenoid and branched glycerol dialkyl glycerol tetraether membrane lipids (iso/brGDGT; see Appendix A for their structures) have allowed the development of several new molecular proxies used in paleoenvironmental reconstruction (e.g., Schouten et al., 2002, 2013; Hopmans et al., 2004; Weijers et al., 2007). Although isoGDGTs can be found in soil (Leininger et al., 2006) and peat (Weijers et al., 2004, 2006), they are generally most abundant in marine and freshwater environments (Sinninghe Damsté et al., 2002; Blaga et al., 2009). Mesophilic isoGDGT-producing Crenarchaeota (e.g., Wuchter et al., 2004), now called Thaumarchaeota (Brochier-Armanet et al., 2008; Spang et al., 2010), are known to occur in most medium to large lakes (Blaga et al., 2009). Since brGDGTs were originally thought to be produced solely in soil and peat (e.g., Hopmans et al., 2004; Weijers et al., 2007; Schouten et al., 2013), the branched vs. isoprenoid tetraether (BIT) index was developed as a proxy for soil organic matter input in marine sediments (Hopmans et al., 2004; Weijers et al., 2009b). BIT expresses the abundance of brGDGTs relative to the isoGDGT crenarchaeol (GDGT V; for structures and nomenclature; see the Appendix A), the characteristic membrane lipid of pelagic Thaumarchaeota (Sinninghe Damsté et al., 2002; Pitcher et al., 2011b). Subsequently, the BIT index was extended to lake sediments (e.g., Verschuren et al., 2009; Wang et al., 2013). However, this application has become complicated by recent indications of brGDGT production within lakes (e.g., Tierney and Russell, 2009; Tierney et al., 2010; Loomis et al., 2011).

Rainfall variability in equatorial East Africa is governed by biannual passage of the Intertropical Convergence Zone (ITCZ), with the intensity of northeasterly and southeasterly monsoons strongly linked to precessional insolation forcing at the multi-millennial timescale (Verschuren et al., 2009), and to El Niño–Southern Oscillation (ENSO) dynamics at the interannual timescale (Wolff et al., 2011). Verschuren et al. (2009) presented a 25 000-year BIT index record for Lake Challa (3°19′ S, 37°42′ E), near Mt. Kilimanjaro, which corresponded well to both known climatic events for the region and the succession of local lake highstands and lowstands evidenced in high-resolution seismic-reflection data. The BIT index was thus interpreted to reflect changes in the amount of soil-derived brGDGTs, associated with variation in the rate of soil erosion that was assumed proportional to rainfall intensity. However, also in Lake Challa, in situ production of brGDGTs has been identified in the water column (Sinninghe Damsté et al., 2009; Buckles et al., 2014) and has been suggested, but not confirmed, in profundal surface sediments (Buckles et al., 2014). This evidence implies that the BIT index may not respond (or at least not directly) to a variable influx of soil organic matter but is rather controlled by the in-lake production of crenarchaeol by Thaumarchaeota (Sinninghe Damsté et al., 2012a). Strong dependence of the BIT index in Lake Challa sediments on crenarchaeol abundance, rather than brGDGT abundance, was also evident in an almost 3-year monthly time series of settling particles (Buckles et al., 2014). The precise mechanism(s) by which the BIT index responds to changes in precipitation has thus remained elusive. Further investigating the issue, we here present a 2200-year record of GDGT distributions in the Lake Challa sediment record with decadal resolution, with the aim to bridge the resolution (and thus information) gap between our time series of sediment-trap data and the 25 000-year climate-proxy record. To this end, we also analyze GDGT distributions in a chronosequence of recent profundal surface sediments.

## 2 Materials and methods

### 2.1 Study site

Lake Challa is a 4.2 $km^2$ crater lake in equatorial East Africa, situated at 880 m elevation in the foothills of Mt. Kilimanjaro. High crater walls (up to 170 m) confine a small catchment area of 1.38 $km^2$, which during periods of exceptional precipitation can enlarge to 1.43 $km^2$ due to activation of a small creek in the NW corner of the lake (Fig. 1). The water budget of this deep lake (92 m in 2005) is dominated by groundwater, which accounts for ca. 80 % of hydrological inputs (Payne, 1970) and is mostly derived from rainfall on the montane forest zone of Mt. Kilimanjaro (1800 to 2800 m elevation; Hemp, 2006). Passage of the ITCZ twice annually results in a short and a long rainy season. "Long rains" occur from March to mid-May, while typically more intense "short

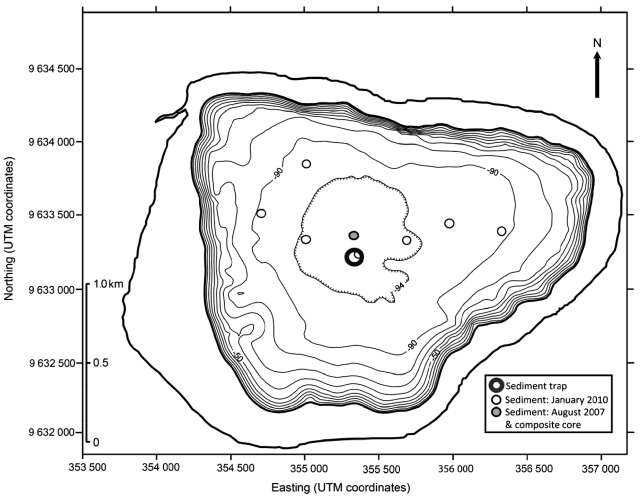


**Figure 1.** Map of Lake Challa and its volcanic crater catchment with bathymetry (Moernaut et al., 2010) and sampling sites relevant to this study: the sediment trap suspended at 35 m water depth, the composite sediment sequence covering the last 2200 years, and intact profundal surface sediments collected in August 2007 (CH07) and January 2010 (CH10). The outermost bold black line denotes the catchment area boundary, which coincides with the crest of the crater rim except in the northwestern corner, where it is breached by a 200 m ravine (see text).

rains" stretch from late October to December (Verschuren et al., 2009; Wolff et al., 2011). Mean daily air temperatures at the lake are lowest (20–21 °C; 24 h average) in July–August (austral winter), and the highest (25–27 °C; 24 h average) in January–February (austral summer; data from 2006 to 2009 provided by A. Hemp, University of Bayreuth; see Buckles et al., 2014). The lake-surface water is coolest (∼ 23 °C) between June and September, promoting seasonal deep mixing that reaches down to 40–60 m depth. During austral summer the surface water can reach 28 °C in the late afternoon, and it experiences shallow daytime stratification followed by wind-driven and convective mixing down to 15–20 m depth (Wolff et al., 2014). The bottom water of Lake Challa is constantly 22.3 °C and permanently anoxic, since it does not mix even on a decadal scale. The finely laminated profundal sediments of Lake Challa (Wolff et al., 2011) contain diatom silica mainly deposited during the cool and windy winter months of deep seasonal mixing (Barker et al., 2011), alternating with organic matter and calcite laminae deposited during the austral spring and summer to produce alternating dark/light layers.

## 2.2 Core collection, sampling, and age model

The composite sediment sequence studied here mostly consists of a mini-Kullenberg piston core (CH03-2K; 2.6 m) recovered in 2003 from a mid-lake location (Fig. 1), supplemented at the top by a cross-correlated gravity core (CH05-1G) and a short section of a Uwitec hammer-driven piston core (CH05-3P-I) recovered in 2005 (Verschuren et al., 2009; Wolff et al., 2011). Importantly, core CH05-1G was kept upright upon retrieval, and its intact sediment–water interface was drained of superfluous water by perforating the transparent core tube shortly below that level. Then, for 2 days, part of its upper interstitial water was allowed to evaporate so as to enable transport without disturbing the fine lamination of recently deposited sediments. The detailed age model for this composite core sequence, which covers the period between ca. 2150 cal yr BP (ca. 200 BCE) and the present (AD 2005) is a smoothed spline through 45 INTCAL09-calibrated AMS $^{14}$C ages of bulk organic carbon, each corrected for an evolving old-carbon age offset determined by paired AMS $^{14}$C dates on charcoal, and supplemented by six subrecent age markers cross-correlated from the $^{210}$Pb-dated gravity core CH99-1G on the basis of shared high-resolution magnetic-susceptibility profiles (Blaauw et al., 2011). This particular core sequence has also been dated through varve counting (Wolff et al., 2011). The latter chronology is fully consistent with the radiometric ($^{210}$Pb, $^{14}$C) chronology, demonstrating that the sediment has been deposited in a continuously anoxic deep-water environment throughout this period. In this study, we examined 208 integrated sediment intervals from 0 to 213 cm depth, each 1 cm (10 mm) thick and sampled contiguously with the exception of five intervals (23–24, 28–29, 99–100, 100–101, and 153–154 cm) where previous analyses had depleted the available material. Each interval of the resulting time series thus represents 10.4 years on average. Throughout this paper, "high-frequency" proxy variations relate to the interannual climate variability as can be resolved by a varved (i.e., annual-resolution) sediment record, and "low-frequency" proxy variations relate to the (multi-)decadal and century-scale climate variability as resolved by our decadal-resolution BIT index time series extracted from the same sediment record. However, this new BIT index record from Lake Challa represents a high-resolution time series when compared to most other lake-based climate-proxy records, in which organic biomarkers tend to be analyzed at a time interval of one data point per century or less.

## 2.3 Organic carbon analysis

Percent organic carbon (%$C_{org}$) data are based on determination of percent organic matter (%OM) at contiguous 1 cm intervals, obtained by the loss-on-ignition (LOI) method (Dean, 1974) and using a linear regression against %$C_{org}$ values obtained on a subset of the same intervals. These %$C_{org}$ values (Blaauw et al., 2011) were determined through combustion of acidified sediment samples on a Fisons NA1500 NCS elemental analyzer (EA) using the Dumas method (courtesy of Birgit Plessen, GFZ-Potsdam). GDGT concentrations reported in this paper are relative to the sample's $C_{org}$ content, unless otherwise stated.

### 2.4 Diatom analysis

Diatom productivity was quantified as the flux of diatom frustules settling in a 58 $cm^2$ sediment trap suspended at 35 m water depth, sampled on a near-monthly basis from 18 November 2006 to 31 August 2010 (i.e., continuously for 45 months in total). For the first 21 months, diatom analysis was performed on one-eighth of the sediment-trap material retained on a GFF filter and preserved frozen until use. This residue was brought back in suspension with distilled water; the filter was rinsed and checked under the microscope for any remaining diatoms. For the remaining 24 months plus one overlapping month (August 2008), diatom analysis was performed on unfiltered but freeze-dried subsamples of the collected sediment-trap material, also brought back in suspension with distilled water. In both cases the suspension containing diatoms was then diluted to a known volume and studied quantitatively at 400× magnification. The 21 samples from December 2006 to August 2008 were pipetted onto a microscope slide and analyzed under an Olympus BX50 microscope with differential-interference contrast. The remaining 24 samples were analyzed under an inverted Olympus CX41 microscope using sedimentation chambers of 10 mL (Uthermöhl, 1931). Total diatom counts were converted to the number of frustules settling per square meter per day. We note that total diatom abundance (and numerical flux) is not linearly proportional to total diatom biomass (and production) at any one time, because the latter also depends on the average cell volume of the species which dominate the community at that time. However, these two sets of variables are broadly proportional to each other at the order-of-magnitude scale of variability observed between successive months and seasons in Lake Challa.

### 2.5 GDGT analysis

Freeze-dried sediments (1–2 g) were extracted with a dichloromethane (DCM) / methanol solvent mixture (9 : 1, $v/v$) using a Dionex™ accelerated solvent extraction (ASE) instrument at high temperature (100 °C) and pressure (1000 psi). Each extract was rotary-evaporated to near dryness and separated by column chromatography using $Al_2O_3$ stationary phase, with the first (apolar) fraction eluted by hexane : DCM (9 : 1, $v : v$) and the second (polar) fraction by DCM methanol (1 : 1, $v : v$). A total of 0.1 µg of $C_{46}$ GDGT standard (see Huguet et al., 2006) was added to the polar fraction. The apolar fraction was archived.

Analysis of the sediment-trap material and recently deposited surface sediments has been described elsewhere (Buckles et al., 2014). Here we report additional results for GDGTs I to IV (see Appendix A) also present in these samples. Sinking particulate matter was sampled at a central location on a near-monthly basis from 18 November 2007 to 31 August 2010, and surface sediments were sampled at seven mid-lake locations in January 2010 (Fig. 1). These samples were processed for GDGT analysis in a slightly different way than core samples (Buckles et al., 2014). In short, the sediment-trap material and surface sediments were extracted using a modified Bligh–Dyer method, yielding both intact polar lipid (IPL) and core lipid (CL) GDGTs. IPL GDGTs were separated from CL GDGTs using column chromatography with an activated silica gel stationary phase, using hexane : ethyl acetate 1 : 1 ($v/v$) and methanol to elute CL and IPL GDGTs, respectively. IPL GDGTs were subsequently subjected to acid hydrolysis to remove the functional head groups and analyzed as CL GDGTs.

Each fraction was dissolved in hexane : isopropanol 99 : 1 ($v : v$) and passed through PTFE 0.45 µm filters prior to high-performance liquid chromatography–atmospheric pressure chemical ionization mass spectrometry (HPLC/APCI-MS). This used an Agilent 1100 series HPLC connected to a Hewlett-Packard 1100 MSD SL mass spectrometer in selected ion monitoring (SIM) mode, using the method described by Schouten et al. (2007). A standard mixture of crenarchaeol : $C_{46}$ GDGT was used to check, and to account for, differences in ionization efficiencies.

GDGT distributions in the samples were quantified using the following indices:

$$\text{BIT index} = \frac{[\text{VIa}] + [\text{VIIa}] + [\text{VIIIa}]}{[\text{VIa}] + [\text{VIIa}] + [\text{VIIIa}] + [\text{V}]}, \quad (1)$$

$$\text{MBT} = \frac{[\text{VIa}] + [\text{VIb}] + [\text{VIc}]}{[\text{all br GDGTs}]}, \quad (2)$$

$$\text{DC} = \frac{[\text{VIb}] + [\text{VIIb}]}{[\text{VIa}] + [\text{VIb}] + [\text{VIIa}] + [\text{VIIb}]}. \quad (3)$$

The fractional abundance of each individual GDGT is expressed as

$$f[\text{GDGT}i] = \frac{[\text{GDGT}i]}{[\Sigma\text{GDGTs}]}, \quad (4)$$

where roman numerals refer to GDGTs in Appendix A; $f[\text{GDGT}i]$ is the fractional abundance of an individual GDGT; $[\text{GDGT}i]$ is the concentration of the individual GDGT, based on surface area relative to the $C_{46}$ standard; $[\Sigma\text{GDGTs}]$ is the summed concentration of all measured GDGTs (I to IIIc); MBT is the methylation index of branched tetraethers; and DC is the degree of cyclization.

The proportion of IPL compared with CL GDGTs is expressed using %IPL, defined as

$$\%\text{IPL} = \left(\frac{[\text{IPL}]}{[\text{IPL}] + [\text{CL}]}\right) \times 100, \quad (5)$$

where [IPL] is the intact polar lipid concentration and [CL] is the core lipid concentration. IPLs represent living, GDGT-producing bacteria/archaea (e.g., Lipp and Hinrichs, 2009; Pitcher et al., 2011a; Schubotz et al., 2009; Lengger et al., 2012).

The measurements of the BIT index were performed in duplicate for all samples; the differences between the two

measurements were on average 0.02. The concentrations of crenarchaeol and the summed acyclic brGDGTs (i.e., VIa + VIIa + VIIIa) were also determined in duplicate.

### 2.6 Statistical analysis

Pearson product-moment correlation coefficients were calculated on unsmoothed time series of the geochemical data at 1 cm interval, using a two-tailed test of significance in IBM SPSS Statistics 21, with bootstrapping at the 95 % confidence interval and missing values excluded pairwise. Calculating mean varve thickness at fixed 1 cm intervals of core depth is complicated, because it requires averaging over a variable number of varves (including partial varves at the start and end of each interval). In addition, the exact boundaries of individual varves can only be discerned microscopically in thin-sectioned sediment, which has inevitably sustained some deformation during its embedding in epoxy. We therefore calculated the correlation between BIT index values and a 9-point running average of annual varve thickness, for varve years most closely matching the mid-depth radiometric age of successive 1 cm BIT index intervals. Due to gaps in the varve-thickness record, and widening of those gaps in the 9-point average time series, this correlation is limited to 159 data pairs. Cut-off values for designation of correlation strengths were based on guidelines by Dancey and Reidy (2004), however with slightly lower boundary conditions allowed to take into account confounding factors such as a relatively large number of GDGT measurements with zero or near-zero values, small but potentially significant time offsets between the calendar-dated varve record and the radiometrically dated geochemical record, the relatively low number of data points in the geochemical time series (208), and ecological factors such as changes in GDGT production (or mean depth of production) and in the influxes of allochthonous materials over time. The strength of (positive/negative) correlation was considered weak if less than 0.3, moderate from 0.3 to 0.5, and strong from upwards of 0.5.

## 3 Results

### 3.1 The 2200-year BIT index record

The percent total organic carbon ($\%C_{org}$) in the composite sediment sequence (Table S1 in the Supplement) varies from 4.4 to 12.5 %, with the lowest values generally grouping between AD 1200 and 1800 (Fig. 2a). The concentration of GDGT-0 (I; see Appendix A) varies widely (97 to 921 $\mu g\, g^{-1}$ $C_{org}$ and standard deviation of 150 $\mu g\, g^{-1}$ $C_{org}$; Table S1), and at an average of 273 $\mu g\, g^{-1}$ $C_{org}$ it is generally high. A baseline concentration of 200–400 $\mu g\, g^{-1}$ $C_{org}$ is interrupted by relatively long-term pulses of > 500 $\mu g\, g^{-1}$ $C_{org}$ (Fig. 2b), the longest of which stretch from around 100 to AD 200, 300 to 500, and 1200 to 1400.

The crenarchaeol ($V$) concentration fluctuates by 2 orders of magnitude between 7 $\mu g\, g^{-1}$ $C_{org}$ at ca. AD 740 and 398 $\mu g\, g^{-1}$ $C_{org}$ at ca. AD 1800 (standard deviation of 64 $\mu g\, g^{-1}$ $C_{org}$; Table S1). Periods of high crenarchaeol (> 150 $\mu g\, g^{-1}$ $C_{org}$) occur from around AD 600 to 650, 1250 to 1300, 1520 to 1570, and 1750 to 1820 (Fig. 2c). The proportion of the crenarchaeol regioisomer (V′) with respect to crenarchaeol ($[V']/([V]+[V'])$) is relatively low and constant at around 2.5 to 3 % throughout the analyzed core sequence (peaking at 4.0 % ca. AD 740; Fig. 2d), confirming that the majority of recovered crenarchaeol originates from aquatic, rather than soil, Thaumarchaeota (cf. Sinninghe Damsté et al., 2012a, b).

The summed concentration of all brGDGTs (relative to $\%C_{org}$) varies by 1 order of magnitude between 95 and 557 $\mu g\, g^{-1}$ $C_{org}$ (standard deviation of 68 $\mu g\, g^{-1}$ $C_{org}$; Table S1). On average, the total brGDGT concentration is higher than that of crenarchaeol (197 vs. 113 $\mu g\, g^{-1}$ $C_{org}$) but similarly displays a baseline (here between 200 and 250 $\mu g\, g^{-1}$ $C_{org}$; Fig. 2e) interspersed by peaks of which the timing generally corresponds to those reported for crenarchaeol. This trend persists when using absolute concentrations in micrograms per gram dry weight. In fact, brGDGT concentrations correlate strongly with crenarchaeol concentrations and those of its regioisomer ($r = 0.67$ and 0.67; Table S2).

The BIT index ranges between 0.42 (101–102 cm; ca. AD 1205) and 0.93 (142–143 cm; ca. AD 740), with an average of $0.65 \pm 0.09$ (Table S1). Generally higher BIT values are evident from ca. AD 650 to 950 (Fig. 2f), followed first by a period of lower BIT values (ca. AD 1170 to 1300) and then a period of higher BIT values (ca. AD 1550 to 1700). Following a 40-year period of very low BIT values (AD 1780–1820), an overall increase to the present is interrupted by two brief periods of lower BIT values, in the late 19th century and in the 1970s. The BIT index does not correlate with the concentrations of any brGDGTs but shows strong negative correlation with the concentrations of crenarchaeol and its regioisomer ($r = -0.70$ and $-0.68$, respectively; Table S2). The BIT index also correlates with measures of brGDGT distribution: moderately positive with MBT ($r = 0.44$) but weakly so with DC ($r = 0.16$; Table S2). MBT values (ranging 0.40 to 0.54) and DC (0.15 to 0.26) themselves do not vary widely (Fig. 3; Table S1).

### 3.2 Settling particles

Results for bulk sediment flux, $\%C_{org}$, crenarchaeol, and brGDGTs in the monthly sediment-trap time series have been presented elsewhere (Sinninghe Damsté et al., 2009; Buckles et al., 2014). Here they are shown (Fig. 4b, d, and e) as reference for new data on the CL and IPL fractions of GDGT-0 (Fig. 4c). Fluxes of IPL GDGT-0 in settling particles are generally low (0.3–0.4 $\mu g\, m^{-2}\, day^{-1}$) from the start of its measurement in December 2007 un-

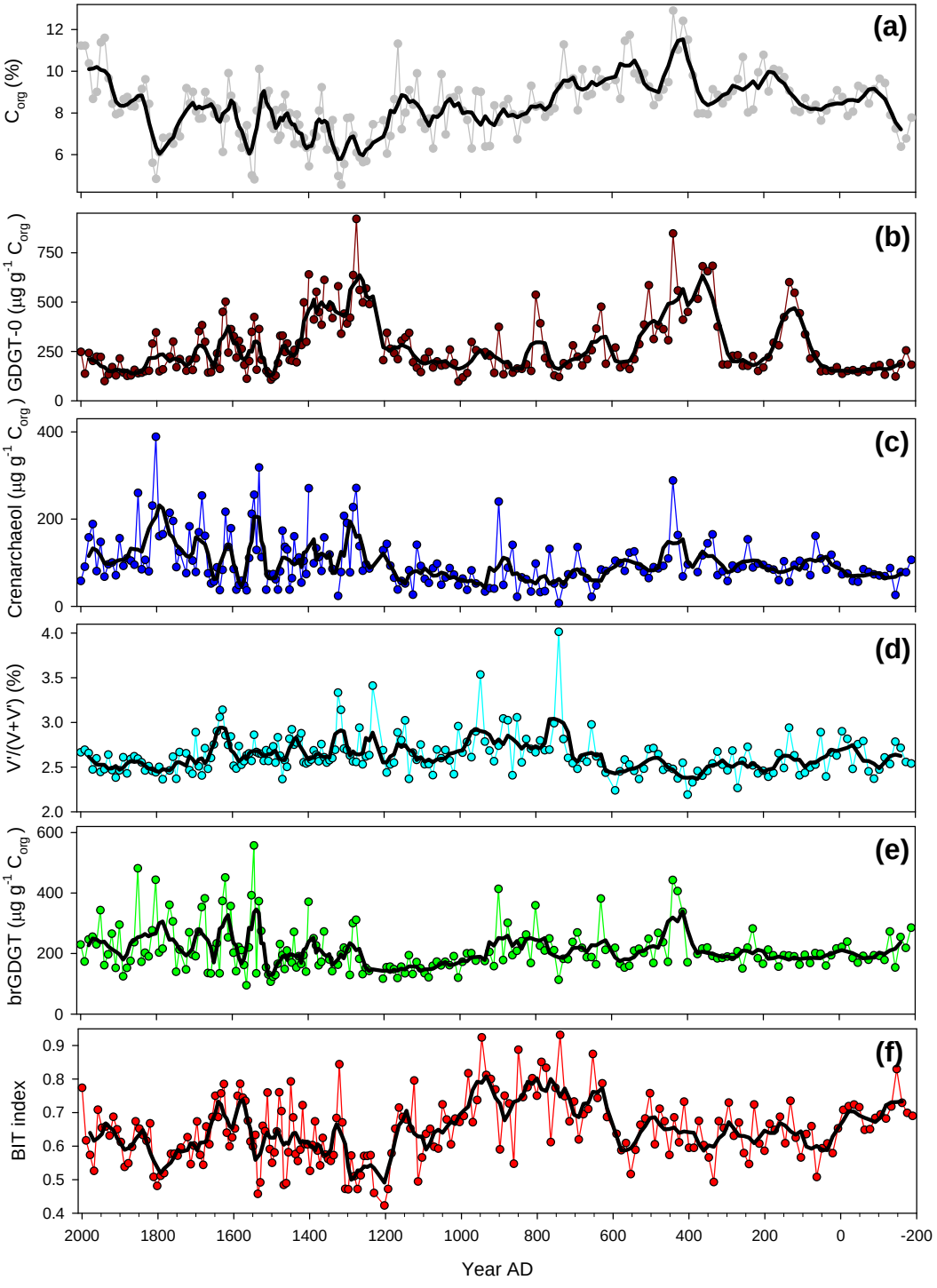


**Figure 2.** Bulk and GDGT parameters in the 213 cm long composite sediment sequence from Lake Challa compared with sediment age in years AD. **(a)** $C_{org}$, **(b)** GDGT-0 concentration, **(c)** crenarchaeol (GDGT-V) concentration, **(d)** the percentage of crenarchaeol regioisomer concentration relative to crenarchaeol, **(e)** summed brGDGT concentration, and **(f)** BIT index. Points connected by a thin line represent raw data and the thicker black lines denote 5-point running averages. A few data points are missing for GDGT concentrations because these were not quantitatively measured.

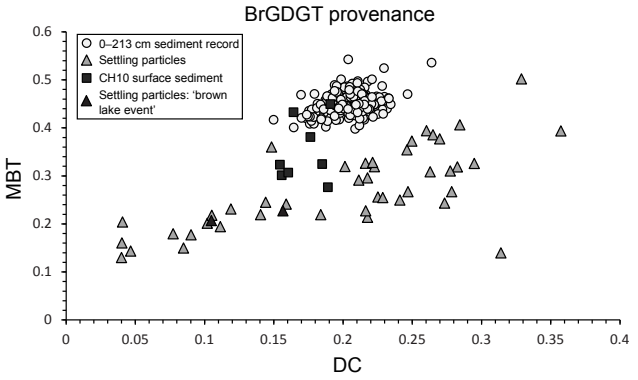


**Figure 3.** MBT vs. DC plot for the 0–213 cm sediment record (circles), for CH10 surface sediments (squares) from Buckles et al. (2014), and settling particles (triangles; data from 18 November 2006 to 1 December 2007 are by Sinninghe Damsté et al., 2009, and data from the following months until 31 August 2010 are by Buckles et al., 2014). Black triangles represent settling particles from March to April 2008, during the episode of intense rainfall when the lake was reported to be turning brown.

til June 2008 (Fig. 4c, Table S3) but subsequently peak at 7.7 µg $m^{-2}$ $day^{-1}$ in August 2008, i.e., during a massive diatom bloom (Fig. 4c). After this maximum, IPL GDGT-0 fluxes vary between 0.0 and 1.7 µg $m^{-2}$ $day^{-1}$, with an additional peak of 2.8 µg $m^{-2}$ $day^{-1}$ in September 2009. CL GDGT-0 fluxes track those of IPL GDGT-0 but are notably lower, ranging from < 0.05 to 2.0 µg $m^{-2}$ $day^{-1}$ (Table S3). From December 2007 to the end of August 2008, IPL GDGT-0 contributes a flux-weighted average of 77 % to total GDGT-0 (Table S4).

### 3.3 Surface sediments

Sinninghe Damsté et al. (2009) and Buckles et al. (2014) presented data on $\%C_{org}$, crenarchaeol (including its regioisomer), GDGT-0, and brGDGTs in Lake Challa surface sediments collected in, respectively, August 2007 (from gravity core CH07-1G: 0–0.5 and 0.5–1 cm depth, here combined into a single result for 0–1 cm labeled CH07) and January 2010 (seven CH10 gravity core tops, all 0–1 cm depth). Here they are shown again (Figs. 5–6) as reference for new data on the 2200-year sediment record and now also include data on IPL and CL GDGT-0 (Tables 1, S5 and S6). IPL and CL GDGT-0 concentrations in CH10 surface sediments are, on average, 14.5 and 8.7 µg $g^{-1}$ dry weight (Table 1). The dominant GDGT in these sediments is GDGT-0, with fractions of 0.85 (IPL) and 0.49 (CL; Fig. 5a; Table 1). Additionally, IPL GDGT-0 represents on average 61 % of total GDGT-0.

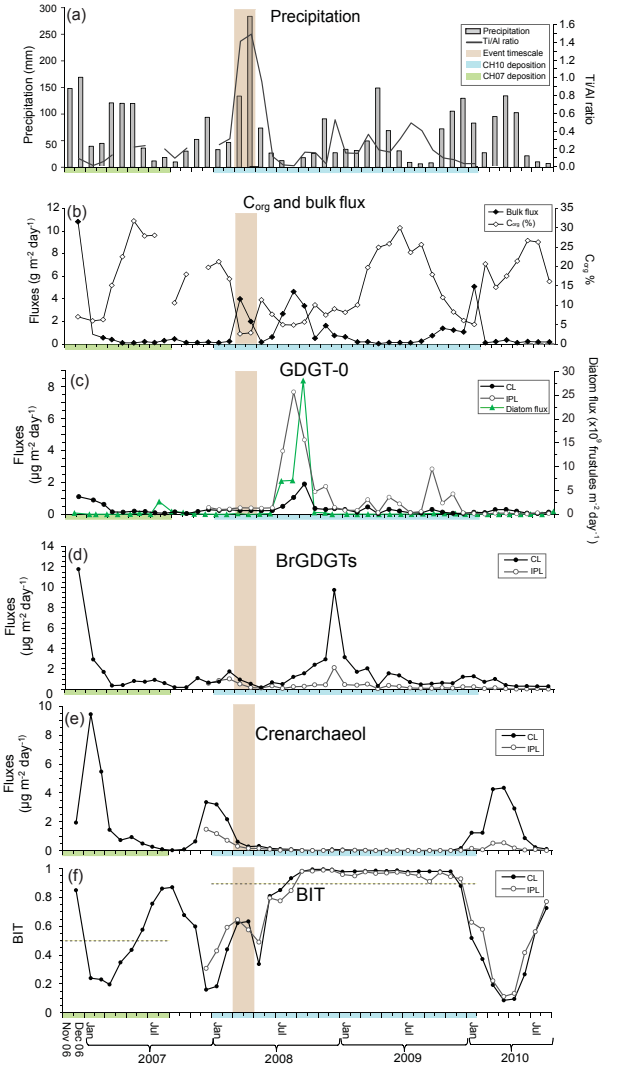


**Figure 4.** Fluxes and GDGT parameters of approximately monthly sediment-trap samples of settling particles, from 18 November 2006 to 31 August 2010. **(a)** Monthly precipitation over the 0.5° × 0.5° grid which includes Lake Challa, from the Global Precipitation Climatology Centre data set, version 6 (GPCC-v6; Schneider et al., 2014), and the Ti / Al ratios of settling mineral particles (Wolff et al., 2014); also indicated are the episodes of heavy rainfall in March–April 2008 and the estimated period covered by the 0–1 cm interval of surface-sediment samples CH07 and CH10. **(b)** Fluxes of bulk sedimenting particles and bulk percent organic carbon ($\%C_{org}$) content. **(c)** Settling fluxes of diatoms and of the IPL and CL fractions of GDGT-0. **(d)** IPL and CL brGDGTs. **(e)** IPL and CL crenarchaeol (GDGT-V). **(f)** IPL and CL BIT index, with dashed horizontal lines representing the average CL BIT indices of surface sediment deposited over the time periods corresponding to CH07 and CH10. In panels **(c)**–**(f)**, geochemical data from 18 November 2006 to 1 December 2007 are by Sinninghe Damsté et al. (2009) and data from the following months until 31 August 2010 are by Buckles et al. (2014).

**Table 1.** Mean ($\pm\sigma$) GDGT concentrations, indices, and distributions in CH10 and CH07 surface sediments. CH07 sediment data are collated from Sinninghe Damsté et al. (2009) and CH10 sediment data are collated from Buckles et al. (2014).

| | Depth interval (cm) | No. of cores | Water depth (m) | | GDGT-0 (μg g$^{-1}$ dry wt.) | Crenarchaeol (μg g$^{-1}$ dry wt.) | Σ[brGDGTs][a] (μg g$^{-1}$ dry wt.) | BIT | MBT | DC |
|---|---|---|---|---|---|---|---|---|---|---|
| CH10 | 0–1 | 7 | 68–92 | IPL | 14.5 (±5.3) | 0.3 (±0.5) | 2.2 (±1.1) | 0.90 (±0.10) | 0.34 (±0.06) | 0.15 (±0.01) |
| | | | | CL | 8.7 (±3.2) | 1.2 (±1.5) | 8.5 (±2.0) | 0.87 (±0.13) | 0.36 (±0.06) | 0.17 (±0.02) |
| CH07 | 0–1 | 1 | 94 | CL | 5.1 | 7.4 | 6.5 | 0.50 | n.m.[b] | n.m. |

| | | | | | Fractional abundance[c] | | | | | | |
|---|---|---|---|---|---|---|---|---|---|---|---|
| | Depth interval (cm) | No. of cores | Water depth (m) | | GDGT-0 (I) | GDGT-1 (II) | GDGT-2 (III) | GDGT-3 (IV) | Crenarchaeol ($V$) | Cren isomer ($V'$) | ΣbrGDGTs[a] |
| CH10 | 0–1 | 7 | 68–92 | IPL | 0.85 (±0.10) | 0.00 (±0.00) | 0.00 (±0.00) | 0.00 (±0.00) | 0.02 (±0.02) | 0.00 (±0.00) | 0.12 (±0.07) |
| | | | | CL | 0.49 (±0.13) | 0.01 (±0.01) | 0.01 (±0.01) | 0.01 (±0.01) | 0.07 (±0.08) | 0.00 (±0.00) | 0.42 (±0.04) |
| CH07 | 0–1 | 1 | 94 | CL | 0.25 | 0.02 | 0.06 | 0.02 | 0.32 | 0.01 | 0.32 |

[a] Sum of brGDGTs VIa, VIIa, and VIIIa; [b] n.m.: not measured; [c] fractional abundances of the GDGT indicated.

## 4 Discussion

### 4.1 Temporal variability in sedimentary GDGT composition and BIT index

The 2200-year, decadal-resolution organic geochemical record of Lake Challa shows a great deal of variation in GDGT composition (Fig. 2b–e), particularly with respect to the concentrations of brGDGTs and crenarchaeol that underpin the BIT index. To allow greater insight into the factors affecting BIT index variation over time, we here quantify the absolute GDGT concentrations, which had not been examined for the 25 000-year, lower-resolution BIT index record (Verschuren et al., 2009; Sinninghe Damsté et al., 2012a). As our 2200-year record is generated from the upper portion of the same composite core sequence, it should show BIT values which are comparable, both in absolute values and variability, to those of the 25 000-year record when the measurements are integrated over identical depth intervals. Indeed, averaging the BIT index values of our new decadal-resolution record over four adjacent 1 cm samples is found to closely mimic the BIT index values obtained from contiguous and homogenized 4 cm sampling increments of the lower-resolution record (Fig. 7). This exercise demonstrates that the lower-resolution record fails to capture strong variation in sedimentary GDGT concentrations (and therefore in the BIT index) on short timescales, as revealed by the high-resolution analysis (Fig. 2b–e). To better understand this high-frequency variability, we first evaluate what can be learned from variability in the present-day system as reflected in the time series of sediment-trap samples and in our chronosequence of surface sediments.

### 4.2 GDGT variability in Lake Challa settling particles and surface sediments

Shared tie points in the visible fine lamination and in magnetic-susceptibility profiles of multiple gravity cores collected between 2003 and 2011 show that the very soft (water content > 95 %) and uncompacted uppermost centimeter

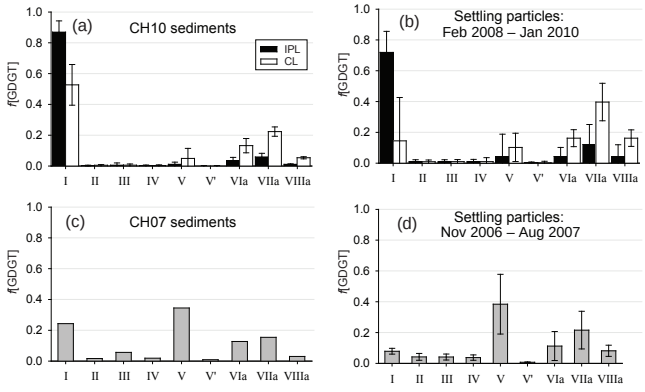


**Figure 5.** IPL and CL GDGT distributions from surface sediments **(a)** CH10 from Buckles et al. (2014) with **(b)** corresponding weighted average IPL and CL GDGT distributions from summed fluxes of settling particles between 30 January 2008 and 30 January 2010, also from Buckles et al. (2014). **(c)** CL GDGT distributions from surface sediment CH07 from Sinninghe Damsté et al. (2009) and **(d)** corresponding weighted average CL GDGT distributions from summed fluxes of settling particles between 18 November 2006 and 24 August 2007.

of mid-lake profundal sediments in Lake Challa represents approximately 2 years of deposition (Sinninghe Damsté et al., 2009; Blaauw et al., 2011). This is also confirmed by $^{210}$Pb dating of the cross-correlated gravity core CH99-1G (see Blaauw et al., 2011, for further details). Consequently, our core-top sample CH07 (0–1 cm) can be treated as broadly representing the period from mid-2005 to August 2007, and CH10 (0–1 cm) the period from early 2008 to January 2010. By comparison, 1 cm of compacted sediments in our 2200-year record represents about a decade of deposition. Note that this is also the case at its very top, because the intact sediment–water interface of core CH05-1G was "compacted" in the field by draining and evaporation of interstitial water in preparation of transport (cf. Sect. 2.2).

GDGTs in CH10 surface sediments are dominated by GDGT-0 and brGDGTs, with relatively low proportions of

crenarchaeol (Fig. 5a). IPL and CL BIT index values are therefore high at ca. 0.90 (Table 1; Fig. 6d). This differs markedly from the CL GDGT composition of CH07 surface sediment. CH07 has a higher proportion of crenarchaeol than either brGDGTs or GDGT-0 (Fig. 5c) and consequently displays a lower BIT index value (0.50; Fig. 6d). This shift in fractional abundances is also reflected in the absolute concentrations (Table 1). The BIT index difference between CH10 and CH07 surface sediments is consistent with BIT index trends in settling particles, which are higher, on average, over the period covered by CH10 than over the period covered by CH07 (Fig. 4f). Whereas 45 months of sediment trapping has yielded BIT index values ranging between 0.09 and 1.00, the absolute difference (0.40) between BIT index values of the temporally more integrated surface-sediment samples CH07 and CH10 is comparable to the full range of BIT index variation in the 2200-year sediment record (Fig. 6d). Our monthly collections of settling particles also yield far greater differences in GDGT distribution (Fig. 4c–f) and brGDGT composition (Fig. 3) than any other sample group. This implies that a still higher-resolution geochemical analysis of a long sediment record would yield even greater temporal variation in GDGT distribution than observed in this study, at least in the case of Lake Challa, where seasonal variation in the composition of settling materials is preserved intact as finely laminated sediments with annual rhythm (varves).

Since the brGDGTs and crenarchaeol found in Lake Challa sediments are thought to be primarily produced between 20 and 40 m depth (Buckles et al., 2013, 2014), it is tempting to attribute these rapid changes in the GDGT composition of descending particles and surface sediments to shifts in the GDGT-producing community within the water column. In Lake Challa, crenarchaeol is produced by Thaumarchaeota that have bloomed annually during the austral summer (between November and February) in three out of four monitored years (Fig. 4e). Its production in the suboxic zone between 20 and 45 m depth (Buckles et al., 2013) is where the majority of GDGTs found in surface sediments originate (Buckles et al., 2014). Thus, data from settling particles trapped at 35 m depth can be used to assess the amounts and distribution of GDGTs exported to the sediments. Here, we examine fluxes of settling particles (Sinninghe Damsté et al., 2009; Buckles et al., 2014) integrated over the time period from November 2006 to August 2007 and from February 2008 to January 2010 (Table 2). Encompassing the 2 years prior to collection of our CH10 surface-sediment samples, the latter period is taken to represent the contribution of GDGTs from the water column to CH10 sediments (0–1 cm depth). The former period encompasses just under a year of deposition prior to collection of CH07 surface sediments and thus does not cover the 2 years of deposition approximately represented by its 0–1 cm interval; however, GDGT compositions of the 0–0.5 and 0.5–1.0 cm intervals of CH07 (analyzed separately; Table S4) are comparable.

Comparison of these two types of time-integrated samples shows, simultaneously, the strong contrast in the distribution of GDGTs exported to Lake Challa sediments during these two time periods (cf. Fig. 5b and d) and the good overall correspondence between GDGT distributions in settling particles and surface sediments that represent the same period (Fig. 5: a–b vs. c–d). GDGT-0 is present in higher proportions in CH10 and CH07 surface sediments than in settling particles (Fig. 5: a–c vs. b–d), likely indicating additional production within the bottom sediments and/or in the water column below 35 m depth (cf. Buckles et al., 2014). BrGDGTs (GDGTs VI–VIII) appear to have similar proportions in sediments and settling particles (accounting for the difference in GDGT-0). However, MBT indices of the two sample groups are slightly offset (Fig. 3). This is most likely due to a (small) contribution from sedimentary brGDGT production, as identified previously by Buckles et al. (2014). Besides these minor differences, the GDGT distributions in settling particles during both periods largely replicate the contrast in GDGT distribution between CH10 and CH07. As the former are due to changes in the GDGT-producing community within the upper part of the water column, we can use our monthly GDGT-flux time series to determine the cause(s) of short-term shifts in sedimentary GDGT distribution.

CL crenarchaeol fluxes in settling particles reached three clear peaks, indicating thaumarchaeotal blooms, in January 2007 ($9\,\mu g\,m^{-2}\,day^{-1}$, Fig. 4e; Table S3), December 2007 to January 2008 ($3\,\mu g\,m^{-2}\,day^{-1}$), and March to April 2010 ($4\,\mu g\,m^{-2}\,day^{-1}$). IPL crenarchaeol fluxes (where available) were an order of magnitude lower than, but covaried with, CL fluxes. IPL GDGT-1, -2, and -3 fluxes covaried with crenarchaeol (Table S3), indicating that they are primarily produced by Thaumarchaeota as previously discussed by Buckles et al. (2014). In contrast, CL brGDGT fluxes peaked at $12\,\mu g\,m^{-2}\,day^{-1}$ between mid-November and December 2006 (Fig. 4d) and at $10\,\mu g\,m^{-2}\,day^{-1}$ in December 2008. Concurrent with maxima in IPL brGDGTs, they are likely due to blooms of brGDGT-producing bacteria in the water column (Buckles et al., 2014). Although both maxima occurred near the end of the short rain season and may thus represent a seasonal bloom, they occurred in only two of four such seasons that we monitored. Since the first peak in brGDGT fluxes occurred during deposition of CH07 and the second during deposition of CH10, this may account for their similar brGDGT concentration (Table 1; Fig. 6c).

GDGT-0 fluxes were high (CL: ca. $1\,\mu g\,m^{-2}\,day^{-1}$; IPL not measured) between mid-November and December 2006 but declined to near-zero values by March 2007 (Fig. 4c; Table S3). GDGT-0 fluxes peaked again in August 2008 (2 and $8\,\mu g\,m^{-2}\,day^{-1}$, respectively, for CL and IPL). During these maxima, crenarchaeol, and cyclic isoGDGTs did not covary with GDGT-0, confirming a separate source for GDGT-0 in the water column as previously suggested (Sinninghe Damsté et al., 2009, 2012a; Buckles et al., 2013).

**Table 2.** Fluxes and indices of GDGTs in settling particles throughout the estimated deposition periods of CH10 and CH07 surface sediments. GDGT data from 18 November 2006 to 1 December 2007 are collated from Sinninghe Damsté et al. (2009) and those from 31 December 2007 to 31 August 2010 are collated from Buckles et al. (2014).

| Settling particles | Deployment date | Collection date | $C_{org}$ (%) | Bulk flux ($g\,m^{-2}\,day^{-1}$) | GDGT-0 ($\mu g\,m^{-2}\,day^{-1}$) | | Crenarchaeol ($\mu g\,m^{-2}\,day^{-1}$) | | Σ[brGDGTs][a] ($\mu g\,m^{-2}\,day^{-1}$) | | BIT | | MBT | | DC | |
|---|---|---|---|---|---|---|---|---|---|---|---|---|---|---|---|---|
| | | | | | IPL | CL | IPL | CL | IPL | CL | IPL | CL | IPL | CL | IPL | CL |
| 2008–2010 (CH10) | 30/01/2008 | 30/01/2010 | 12.5 | 1.3 | 1.3 | 0.3 | 0.1 | 0.2 | 0.4 | 1.6 | 0.86 | 0.86 | 0.29 | 0.28 | 0.17 | 0.20 |
| 2006–2007 (CH07) | 18/11/2006 | 24/08/2007 | 18.1 | 1.5 | n.m.[b] | 0.4 | n.m. | 2.3 | n.m. | 2.3 | n.m. | 0.50 | n.m. | 0.25 | n.m. | 0.18 |

[a] Sum of brGDGTs VIa, VIIa, and VIIIa; [b] n.m.: not measured.

Microbiological analysis of suspended particulate matter (SPM) from Lake Challa collected in February 2010 (Buckles et al., 2013) yielded no evidence of methanogens or other anaerobic archaea in the upper 35 m of the water column, in line with the near-zero fluxes of GDGT-0 in settling particles trapped at this time (Fig. 4c). However, in SPM from anoxic waters deeper down, Buckles et al. (2013) found high concentrations of GDGT-0. Based on 16S rRNA sequence data, its source was identified as the uncultured archaeal group 1.2 (also named C3 by DeLong and Pace, 2001) and the "miscellaneous Crenarchaeota group" (MCG, also referred to as group 1.3; Inagaki et al., 2003). Presence of these archaeal sequences in the permanently stratified lower water column during a single sampling of SPM does not prove the origin of similar isoGDGT distributions in settling particles from the suboxic zone 2 years previously. Comparison with denaturing gradient gel electrophoresis (DGGE) performed on Lake Challa SPM taken in September 2007 (Sinninghe Damsté et al., 2009) shows that archaea in the anoxic water column also mostly fall in group 1.2 and the MCG (MBG-C) group of the Crenarchaeota, as well as showing contributions from Halobacteriales of the Euryarchaeota.

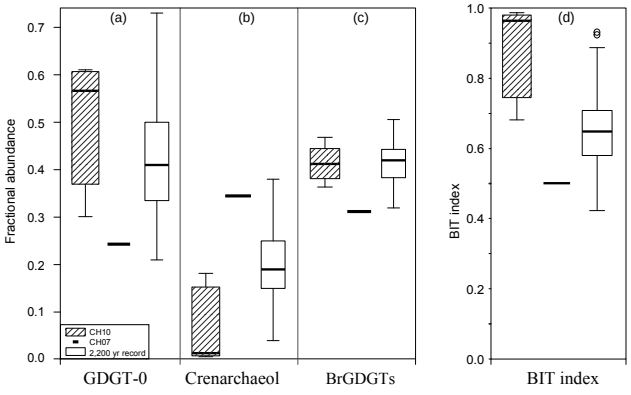


**Figure 6.** Box plot of fractional abundances of **(a)** CL GDGT-0 (I), **(b)** CL crenarchaeol V, **(c)** CL summed brGDGTs, and **(d)** the BIT index for surface sediments CH10 ($n = 7$, 0–1 cm depth) collated from Buckles et al. (2014), CH07 collated from Sinninghe Damsté et al. (2009), and the 2200-year sediment record (0–213 cm depth at 1 cm resolution, where 1 cm represents on average 10.4 years of deposition). Note that surface sediments represent 2–3 years of deposition. The box corresponds to the interquartile range and the whiskers extend to 1.5 times the length of the box (unless the full range of data is smaller than this); outliers are defined here as being outside the maximum extent of the whiskers. The black horizontal line inside the box represents the median.

### 4.3 Effect of a soil-erosion event on the GDGT-producing community

The occurrence of a short-lived influx of allochthonous material in March–April 2008 provides a potential explanation for the change in the GDGT-producing community of Lake Challa that caused the dramatic shift in GDGT composition between CH07 and CH10 surface sediments.

Material settling in Lake Challa from March to May 2008 displayed a singularly large peak in the molar ratio of titanium to aluminum (Ti / Al; Fig. 4a), a tracer for detrital mineral sediment components (Weltje and Tjallingii, 2008; Wolff et al., 2014). This Ti / Al peak is unprecedented in the Lake Challa sediment-trap record and coincided with a peak in bulk settling flux (4.0–2.0 $g\,m^{-2}\,day^{-1}$), low OM content (3 % $C_{org}$; Fig. 4b), and local reports of the lake "turning brown", all pointing to enhanced allochthonous input to the lake triggered by the onset of the principal rain season that year (Fig. 4a). The likely source of this material is loose topsoil on and beyond the NW rim of Challa crater, mobilized during particularly intense precipitation and carried to the lake by the (usually) dry creek which breaches the rim there (Fig. 1). Notably, the brGDGT distributions and abundances in particulate matter settling during these months were not discernibly affected by soil-derived brGDGTs, most probably due to the high background flux of lacustrine brGDGTs and the low OM content of the eroded soil (Buckles et al., 2014; Table S3). If this soil-erosion event did cause the observed shift in Lake Challa's GDGT-producing community, its effect must have been indirect.

Nutrients triggering the annual diatom bloom in Lake Challa during austral winter (July–August; see Sect. 2.1) are generally sourced from its anoxic, nutrient-rich lower water column by wind-driven seasonal mixing (Wolff et al., 2011, 2014; Barker et al., 2013). In the austral winter of 2008, seasonal mixing began as early as June and re-establishment of stratification was slow (Wolff, 2012; Buckles et al., 2014; Wolff et al., 2014). However, the massive diatom bloom of July–September 2008 (far larger than any other in our 4-year

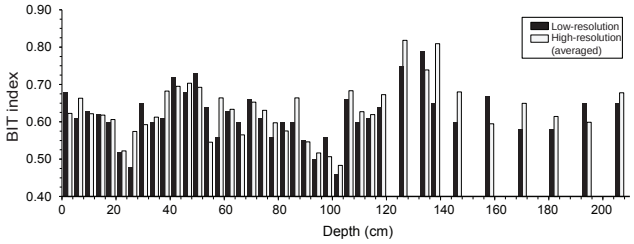


**Figure 7.** Comparison of BIT index values from our decadal-resolution time series, averaged over four adjacent 1 cm sections, against the BIT index measured on integrated 4 cm sections of the same sediment core analyzed earlier by Verschuren et al. (2009).

time series; Fig. 4c) peaked during the early months of deep seasonal mixing. Therefore, the extended period of nutrient advection that year is unlikely to have been the main cause of this particularly abundant diatom bloom. We hypothesize that additional, soil-derived (micro)nutrients delivered during intense rainfall between March and May 2008 may have been the primary driver for the unusually large diatom productivity later that year. Nutrients released by the decomposition of soil organic material in the lake would amplify the (annual) 2008 austral-winter diatom bloom (Fig. 4c; Wolff et al., 2011).

Considering that the coincident peak flux of GDGT-0 is especially clear in the IPL lipids (Fig. 4c), and considering the position of the sediment trap in the suboxic portion of the water column, we tentatively infer that a GDGT-0-producing community of archaea (specifically Euryarchaeota) developed at the oxic–suboxic transition below the euphotic zone and was likely involved in the degradation of dead, settling diatoms as the austral-winter bloom reaches its peak. Alternatively, as a result of the unusually high oxygen demand of the 2008 diatom bloom, the oxycline may have temporarily ascended. This would have resulted in the presence of GDGT-0-producing archaea above the sediment trap and their signal being captured by the collection of descending particles at 35 m water depth. This specific condition most likely resulted in the high proportion of GDGT-0 in CH10 sediments (Fig. 5a). The peak in GDGT-0 flux during austral summer 2008 is followed by a subsequent peak in the flux of the brGDGTs (Fig. 4c–d), suggesting that the suboxic niche occupied by GDGT-0-producing archaea was subsequently occupied by brGDGT-producing bacteria (Buckles et al., 2013, 2014). Although little is known about the ecology or even identity of brGDGT-producing bacteria (Weijers et al., 2009a; Sinninghe Damsté et al., 2011, 2014), the occurrence of a similar brGDGT peak in December 2006 (Sinninghe Damsté et al., 2009; Fig. 4c), i.e., following the austral-winter diatom bloom of 2006 (Wolff et al., 2014), suggests that brGDGT-producing bacteria may also thrive on diatom degradation products. This would fit with compound-specific carbon isotopic analyses of brGDGTs in soil (Weijers et al., 2010; Oppermann et al., 2010), which suggest that brGDGT producers are heterotrophic bacteria. Indeed, brGDGTs and structurally related membrane lipids have so far only been identified in heterotrophic Acidobacteria (Sinninghe Damsté et al., 2011, 2014).

Most notably, however, Thaumarchaeota did not thrive during the 2008/2009 austral summer (Fig. 4e) which followed the massive diatom bloom, and this most likely accounts for the low crenarchaeol abundance in CH10 surface sediments compared to CH07 (Fig. 5b). Since Thaumarchaeota are nitrifiers (Könneke et al., 2005; Wuchter et al., 2006), they should in principle have prospered on the ammonium released by the degradation of algal biomass from the austral-winter diatom bloom. In fact, North Sea studies have shown that Thaumarchaeota blooms follow phytoplankton blooms in that setting (Wuchter et al., 2006; Pitcher et al., 2011c). However, the abundant ammonium generated by the massive diatom bloom of July–September 2008 may have disturbed the competition between nitrifying archaea and bacteria. As nitrifying bacteria have a competitive advantage over nitrifying archaea at higher ammonium levels (Di et al., 2009) and vice versa (Martens-Habbena et al., 2009), high ammonium concentrations may have suppressed the Thaumarchaeota and resulted in the absence of a normally quasi-annual crenarchaeol bloom during the 2008–2009 austral summer (Fig. 4e).

### 4.4 Connection between the BIT index and precipitation

Before the discovery of substantial in situ brGDGT production in Lake Challa (Buckles et al., 2014), it was thought that precipitation-triggered soil erosion transported soil-derived brGDGTs into the lake and settled in the sediments against a background of aquatic crenarchaeol, thus increasing the BIT index (Sinninghe Damsté et al, 2009; Verschuren et al., 2009). Since soil-derived brGDGTs entering Lake Challa during March–May 2008 did not discernibly affect the brGDGT distributions and abundances in particulate matter settling at that time (Buckles et al., 2014), the event is barely registered in the BIT index of those settling particles (Fig. 4f). Therefore, how does this evidence support the use of the sedimentary BIT index as a hydroclimatic proxy in this system (Verschuren et al., 2009)?

Variation in the relative proportions of crenarchaeol and brGDGTs in the 25 000-year sediment record (Sinninghe Damsté et al., 2012a) had already indicated that variability in crenarchaeol is the main driver of BIT index changes in Lake Challa. Also in the higher-resolution record studied here, the BIT index correlates (negatively) with the concentration ($\mu g\, g^{-1}\, C_{org}$) of crenarchaeol ($r = -0.69$) and its regioisomer ($r = -0.68$) but does not correlate significantly with brGDGT concentration (Table S2). Thus, the sedimentary BIT index variations must be caused primarily by variation in crenarchaeol production and, consequently, by the strength of the thaumarchaeotal bloom in austral summer.

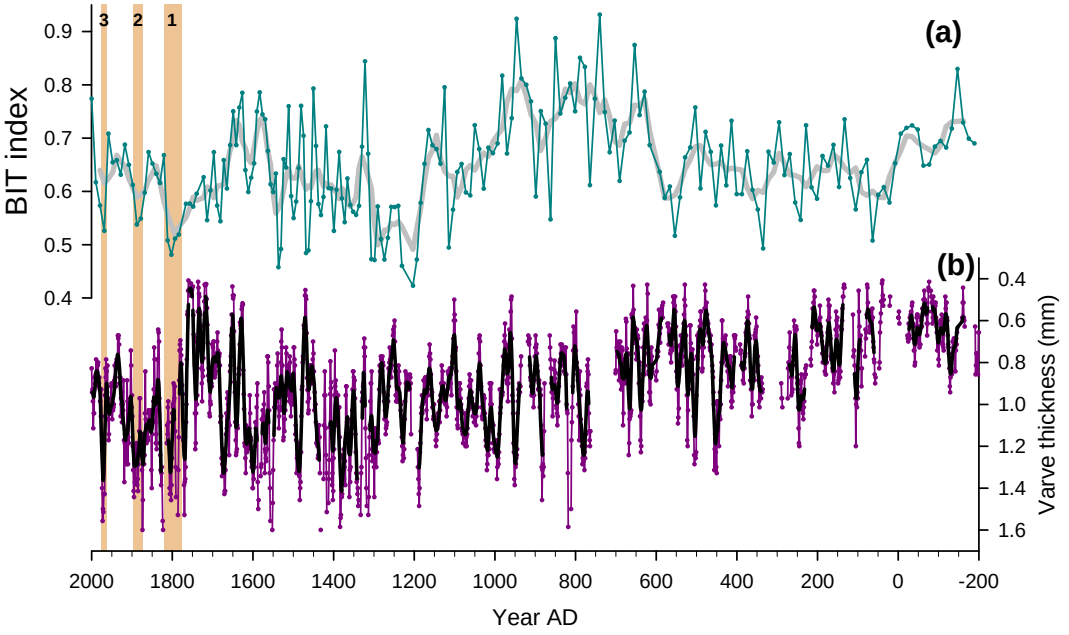


**Figure 8.** **(a)** Decadal-resolution time series of BIT index variability in the 2200-year sediment record from Lake Challa, with black symbols and lines representing the raw data and the thick grey line a 5-point running average. **(b)** Time series of varve thickness in the same record (Wolff et al., 2011), with purple symbols and lines representing the raw data and the thick black line a 9-point running average. Orange-shaded bars highlight the approximate duration of documented periods of drought in East Africa (see text): (1) 1780–1820, (2) 1870–1895, and (3) AD 1968–1974.

Extrapolating from the observation by Wolff et al. (2011) that years with stronger austral-winter winds in the Lake Challa area tend to be associated with a weak southeasterly monsoon compromising the principal rain season (March–May), Sinninghe Damsté et al. (2012a) formulated a mechanism potentially explaining the generally positive match between the BIT index and the seismic-reflection evidence for climate-driven lake-level changes in Lake Challa over the past 25 000 years (Verschuren et al., 2009). Stronger wind and its lake-surface cooling result in deeper mixing, both enhancing the regeneration of nutrients from the lower water column to the photic zone and delaying the recovery of water-column stratification, in turn producing larger diatom blooms in drier years. The ammonium released by this decaying diatom organic matter promotes greater proliferation of Thaumarchaeota and production of crenarchaeol. As a result, drier years tend to produce lower BIT indices than wetter years. Over the multi-millennial timescale considered by Sinninghe Damsté et al. (2012a), conditions of high lake level and more stable water-column stratification during relatively wet climate episodes were envisioned to have limited the proliferation of Thaumarchaeota, compared to dry lowstand episodes with less stable water-column stratification and, hence, greater in-lake nutrient regeneration to the photic zone.

Results from our monitoring program of Lake Challa, however, now point to a possible second mechanism generating high BIT index values during episodes of generally wetter climate conditions. We propose that, in this permanently stratified and (most often) unproductive tropical lake, episodic injection of extra nutrients derived from the catchment soils eroded during intense rainfall starts a cascade of events eventually leading to the replacement of nitrifying archaea (Thaumarchaeota) by nitrifying bacteria, and thus reduction of crenarchaeol deposition (cf. Fig. 6b), resulting in high BIT index values (Fig. 6d). We postulate that the strongly seasonal nature of Thaumarchaeota proliferation in this system, and dependence of these Thaumarchaeota on the suboxic niche in the water column (Buckles et al., 2013), leaves them more vulnerable to such episodic events. According to this mechanism, the BIT index can be considered to reflect the frequency of "extreme" soil-erosion events, which in this semiarid region have a positive, but threshold-controlled, relationship with rainfall. As is typical for a semiarid tropical climate regime, cumulative total annual rainfall in the Lake Challa area mostly results from a relatively limited number of high-intensity precipitation events, concentrated in but not limited to the principal rain-season months. Past periods with a wetter climate (higher mean annual rainfall) can thus be expected to have been characterized by a greater frequency of precipitation events sufficiently intense to cause significant erosion of catchment soils. Either alternatively or simultaneously, these wet periods may also have been characterized by a level of seasonal soil-water satura-

tion sufficient to markedly lower the threshold for soil erosion when hit by intense rainfall. In conclusion, we note that both of the above mechanisms provide a feasible explanation for how high precipitation generates high BIT index values. Which of these mechanisms has a dominant influence on sedimentary BIT index variations may depend primarily on the timescale of the analysis.

### 4.5 A high-resolution record of monsoon precipitation

Wolff et al. (2011) produced a 3000-year record of (submillimeter-scale) varve-thickness variation in Lake Challa bottom sediments using the same composite sediment sequence that we analyzed at 1 cm resolution (Fig. 8b), and showed that the thicknesses of varves deposited over the last 150 years correlate both with indices of ENSO (Niño3.4 SST and the Southern Oscillation index: Ropelewski and Jones, 1987; Kaplan et al., 1998) and with sea surface temperature (SST) anomalies averaged over the western Indian Ocean (Rayner et al., 2003). Specifically, thick varves are deposited during prominent La Niña years, during which East Africa tends to experience anomalous drought, and thin varves tend to correspond to El Niño years, which are often characterized by high rainfall. Noting that most of the varve-thickness variation resides in variation of the light laminae, which are mainly composed of diatom frustules, Wolff et al. (2011) proposed that prolonged dry and windy conditions during the austral-winter season of La Niña years promote the deep water-column mixing required to supply surface water with adequate nutrients for diatom growth. As a consequence, La Niña conditions create more prominent annual diatom blooms and thus result in thicker varves. Lake Challa varve thickness thus appears to be an indicator of the portion of interannual rainfall variability in East Africa that is under control of its teleconnection with ENSO, with greatest sensitivity for the anomalously dry conditions typical of La Niña events.

Wolff et al. (2011) also noted broad visual agreement between (multi-)decadal trends in the Challa varve-thickness record (represented by its 21-point running average) and the last 3000 years of the low-resolution Challa BIT index record (Verschuren et al., 2009), and similarly between a 7-point running average of the Challa varve-thickness record and a 1100-year moisture-balance reconstruction from Lake Naivasha in central Kenya (Verschuren et al., 2000), 400 km northwest of Lake Challa. Broad correspondence between the hydroclimatic histories of lakes Challa and Naivasha is not unexpected, since both sites are located within the broader "Horn of Africa" region of coastal East Africa, where (multi-)decadal variation in monsoon rainfall is strongly tied to SST changes in the Indian Ocean (Tierney et al., 2013). More importantly, this correspondence seems to imply that a substantial part of the (multi-)decadal variation in this region's monsoon rainfall can be attributed to the compound effect of alternating increases and decreases in the frequency of La Niña events, possibly mediated by changes in the regional geometry of atmospheric convergence (i.e., ITCZ migration; Wolff et al., 2011) and/or Indian Ocean SST patterns. However, the mechanisms of external climate forcing known to influence ENSO dynamics at these longer timescales (solar irradiance variation, temporal clustering of volcanic activity; Mann et al., 2005) may also, and simultaneously, exert a direct influence on Lake Challa diatom productivity, for example through temperature effects on the seasonal cycle of water-column mixing and stratification. Importantly, this direct influence is not necessarily synchronized with or even of the same sign as the relationship between varve thickness and rainfall at the interannual timescale. This complexity of proxy-signal attribution warrants caution in the extraction of multi-decadal and century-scale rainfall trends from the Challa varve-thickness record, and leaves room for other sediment-derived proxies with the appropriate sensitivity and range of variation to more reliably capture these longer-term trends in the region's hydroclimate.

Focusing on such (multi-)decadal hydroclimate variability within the last two centuries, both our decadal-resolution BIT index record and the Challa varve-thickness record are highly congruent with independent historical data and previously available climate-proxy records from equatorial East Africa. The most prominent negative excursion in the BIT index time series within this period, here dated to between AD $1779 \pm 14$ and $1816 \pm 11$ and consisting of four consecutive data points with BIT index values of 0.48–0.52 (Fig. 8a), matches the episode of extreme aridity that ended the region's generally moist Little Ice Age climate regime (Verschuren and Charman, 2000). In most paleoclimate records employing an age model based on a combination of $^{14}$C and $^{210}$Pb dating (Verschuren et al., 2000; Stager et al., 2005; Bessems et al., 2008; Kiage and Liu, 2009; De Cort et al., 2013), this dry episode is situated sometime during the late 1700s to early 1800s. High-resolution $^{210}$Pb dating on the sediment record from Lake Sonachi near Naivasha had earlier constrained the end of this drought to AD $1815 \pm 8$ (Verschuren et al., 1999), i.e., indistinguishable from our age estimate for the end of the prominent BIT anomaly at Lake Challa. Within analytical and age-modeling error, both of these radiometric ages are also indistinguishable from the date of AD 1822–1826 on a prominent Ba / Ca peak in a coral from Kenya's Indian Ocean coast (Fleitmann et al., 2007), which is inferred to reflect increased soil runoff from the Sabaki River catchment caused by drought-breaking flood events.

A second prominent BIT index minimum at Lake Challa, consisting of two data points with values of 0.54–0.55 dated to between AD $1873 \pm 7$ and $1893 \pm 6$ (Fig. 8a), matches diverse historical evidence for a prolonged late 19th century episode of anomalous drought throughout East Africa (Nicholson et al., 2012). In lake-based climate records from Kenya's Rift Valley region, this drought is dated to between the 1870s and early 1890s (Verschuren, 1999; Verschuren et

al., 1999, 2000; De Cort et al., 2013). In agreement with the Challa BIT index time series, historical and proxy evidence from throughout the region indicate that this drought ended in the late 1880s or early 1890s, with generally much wetter conditions prevailing at the very end of the 19th century and the first decades of the 20th century (e.g., Verschuren et al., 1999; Nicholson and Yin, 2001; Verschuren, 2004; Nicholson et al., 2012).

Unresolved data-quality issues concerning the few historical and/or active rain-gauge stations in the wider Challa region preclude a detailed comparison of either the Challa BIT index or varve-thickness records with the instrumental record of annual-mean rainfall at this time, and are beyond the scope of this study. Here we only highlight the exact match between a third BIT index minimum, dated to between AD $1963 \pm 2$ and $1974 \pm 2$ (Fig. 8a), and the cluster of seven thick varves (each of which exceeds 1.4 mm in thickness; Fig. 8b) deposited during a period of near-continuous strong La Niña conditions between 1968 and 1974 (Niño3.4 SST; Kaplan et al., 1998).

Strong visual agreement between the Challa BIT index and varve-thickness records during these three subrecent drought periods is supported by the significant inverse linear correlation between BIT index values and a 9-point running mean of varve-thickness values over the period AD 1800–2000 ($r = -0.55$; $n = 18$). However, this general agreement between the two hydroclimate proxies is not sustained through the earlier part of the record, so that we find no correlation between them for the entire 2200-year period analyzed in this study ($r = -0.09$; $n = 159$). One obvious difference between the two proxy records is their degree of variance over the entire record compared to that during the "historical" part of the record (i.e., the period AD 1780–2005). For the annually resolved varve-thickness record, these variances are respectively 0.046 and 0.061 (a ratio of 1.33), whereas for the high-resolution ($\sim 10$ years) BIT index record these variances are respectively 0.0053 and 0.0088 (a ratio of 1.68). This is so because the varve-thickness time series, with the exception of a cluster of thin (< 0.6 mm) varves deposited during the early 18th century, mostly displays a single trend of gradually increasing thickness throughout the 2200-year record, with lower-frequency variability not much greater (or more extreme) than that realized during the last two centuries. The BIT index time series, in contrast, displays several pronounced fluctuations at the (multi-)decadal and century timescale, with minima and maxima inferring the occurrence of past hydroclimatic conditions during the past 2200 years that were both substantially drier and wetter than the historical extremes. Specifically, the Challa BIT record is consistent with the general temporal pattern of East Africa's climate history during the last millennium, which features a medieval period of prolonged aridity (here, the driest episode is dated to AD 1170–1300) followed by generally wetter conditions during the East African equivalent of the Little Ice Age (Verschuren, 2004; Verschuren and Charman, 2000; Tierney et al., 2013).

According to our Challa BIT index record, easternmost equatorial Africa enjoyed its wettest period of the last 2200 years between ca. AD 600 and 1000 (Fig. 8a). Although quite variable in its expression among the set of presently available records, a distinct period of inferred higher rainfall occurring towards the end of the first millennium AD has also been reported from several other lakes across East Africa: Lake Naivasha in central Kenya reached peak lake level (and minimum salinity) around AD 900 (Verschuren et al., 2000; Verschuren, 2001), and low %Mg values in sedimentary carbonates from Lake Edward in western Uganda infer a positive moisture balance between AD 900 and 1000 (Russell and Johnson, 2007). Given large uncertainty on the timing of this episode in most East African lake-based climate records (at least compared to Lake Challa), the reported proxy signatures may well represent the same, and region-wide, event of elevated rainfall. The first half of the first millennium AD appears to have been rather dry by comparison (mean BIT index value $0.63 \pm 0.06$ SD (standard deviation), $n = 45$; Fig. 8a), following generally wet conditions during the second half of the first millennium BCE (mean BIT index value $0.71 \pm 0.04$ SD, $n = 17$; Fig. 8a and Verschuren et al., 2009). Finally, the timing of the abrupt drying trend which forms the transition between these two contrasting climate states, here dated to between 45 BCE and AD 57 (AD $7 \pm 50$; Fig. 8a), matches that of a century-scale episode of pronounced aridity near the start of the Common Era that has been documented from several other East African lakes whose hydroclimatic history has appropriate late-Holocene age control: Naivasha (shortly before the 2nd century AD; Verschuren, 2001), Edward (1st century AD; Russell and Johnson, 2005), and two crater lakes in western Uganda (early 1st century AD; Russell et al., 2007).

The combined evidence on East Africa's hydroclimate variability during the last two millennia, as well as excellent agreement between BIT index minima and prominent episodes of regional drought within the last 250 years, suggests that our high-resolution, and well-dated, BIT index time series from Lake Challa represents a trustworthy reconstruction of multi-decadal and century-scale trends in the hydroclimatic history of easternmost East Africa. This conclusion, together with the contrasting character of the long-term variability displayed by the BIT index and varve-thickness records, supports our proposition that the Challa BIT index is principally a proxy for the region's monsoon precipitation. However, this is so only on timescales long enough to average out the occurrence of relatively infrequent, rainfall-driven soil-influx events that were sufficiently massive to affect the community structure of aquatic microbes, and hence the balance of GDGTs deposited in finely laminated profundal sediments. This is true on (multi-)decadal and century timescales, and up to millennia as long as the general boundary conditions of this climate-recording system have

remained the same. In this context, we note that, even in the "very wet" early Holocene African Humid Period (Gasse, 2000), this region's climate regime was still semiarid with pronounced alternation of wet and dry seasons and an overall deficit of precipitation against evaporation (Verschuren et al., 2009). However, the mechanism by which the climate parameter of interest (here, precipitation) is translated into variability of a climate-sensitive sedimentary proxy is contingent upon site-specific conditions: permanent stratification of the lake's lower water column (creating a permanent but shifting oxycline), dominance of in situ-produced brGDGTs, the strongly seasonal rainfall of high intensity, and the resultant intermittent mobilization of soil from a semiarid tropical landscape. While these conditions appear to make the BIT index an effective precipitation proxy at Lake Challa, we recommend its application to other lakes only when factors controlling the crenarchaeol production by Thaumarchaeota as well as brGDGT production are well understood.

## 5 Conclusions

Catchment soil materials transported to Lake Challa by intense precipitation between March and May 2008 stimulated diatom productivity during the subsequent dry season of July–September 2008 and set in motion a sequence of events that shifted the composition of GDGTs exported to profundal bottom sediments. It included a suppression of the seasonal Thaumarchaeota bloom and thus reduced the production of crenarchaeol, in turn reflected in high BIT index values (i.e., approaching 1) of settling particles and recently deposited profundal sediments. Similarly, variation in the sedimentary BIT index over the past 2200 years results from fluctuations in crenarchaeol production against a background of high in situ brGDGT production. Integrated over approximately 10-year intervals, the magnitude of this BIT index variation is smaller than that observed in the 45-month long time series of settling particles, but similar to that observed between two sets of recent surface sediments collected before and after the episode of Thaumarchaeota suppression. Multi-decadal to century-scale trends in our high-resolution BIT index time series show no significant correlation with those in the annually resolved rainfall reconstruction based on varve thickness, but they do capture the three most prominent known episodes of prolonged regional drought during the past 250 years and are broadly consistent with the hydroclimatic history of East Africa of the last two millennia as presently known.

We propose that the BIT index value of Lake Challa sediments is primarily controlled by variation in the annual Thaumarchaeota bloom during the austral summer, which is suppressed when excess nutrient input associated with occasional rainfall-driven soil-erosion events result in these Thaumarchaeota being outcompeted by nitrifying bacteria. Whereas such rainfall-triggered events of Thaumarchaeota suppression may occur rather infrequently at the interannual timescale, we surmise that their probability of occurrence is enhanced during longer episodes of higher mean annual rainfall, and reduced during longer episodes of relative drought, such that a temporally integrated BIT index record reflects multi-decadal and longer-term trends in local rainfall. Because marked decade-scale maxima and minima in sedimentary BIT index are smoothed further by integration over longer intervals, this mechanism relating the BIT index to rainfall may also apply to the 25 000-year BIT index record from Lake Challa (Verschuren et al., 2009; Sinninghe Damsté et al., 2012a), in which each data point represents a mean BIT index value over ca. 40 years at approximately 160-year intervals. We conclude that the BIT index of Lake Challa sediments reflects the amount of monsoon precipitation indirectly, as is also the case with varve thickness (Wolff et al., 2011) and many other hydroclimate proxies extracted from lake sediments. Prior to application elsewhere, we strongly recommend ascertaining the local situation of lacustrine brGDGT production and of variables affecting the productivity of Thaumarchaeota.

## Appendix A

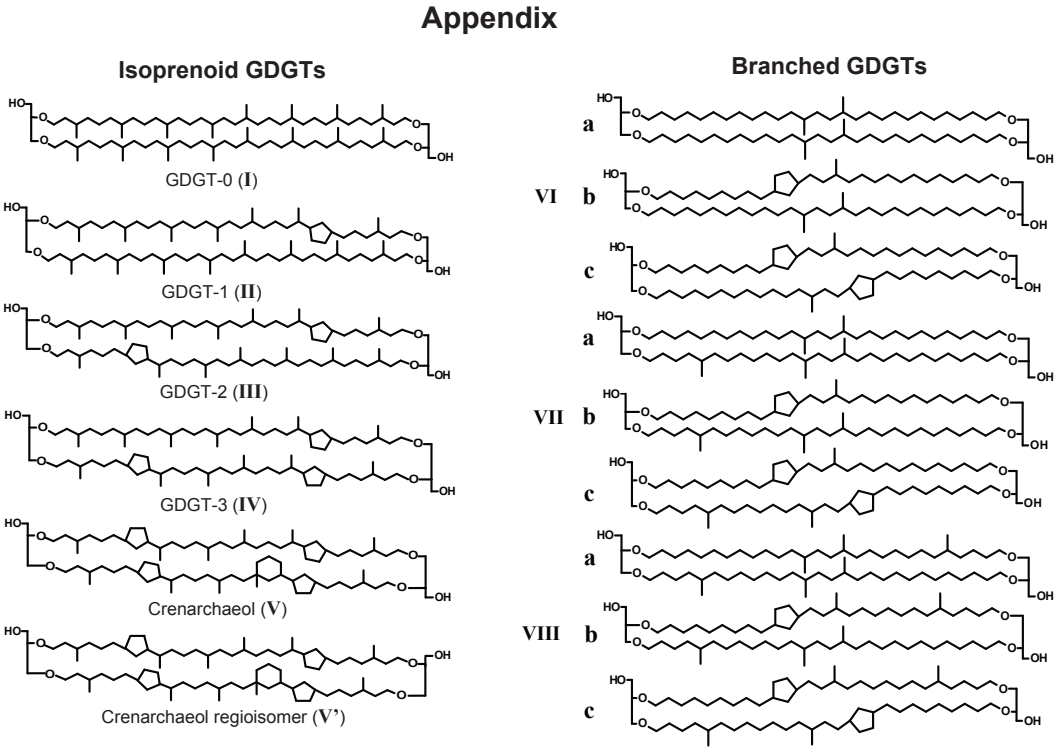


**Figure A1.** Key to GDGT structures. The number of cyclopentane moieties in the isoprenoid GDGTs is indicated by the number following GDGT as indicated. This is not used for crenarchaeol ($V$) and its regioisomer ($V'$) since these GDGTs contain a cyclohexane ring. BrGDGTs are subdivided by their principal number of methyl substituents: four (VI), five (VII), or six (VIII). Each group consists of the parent brGDGT **(a)** and brGDGTs with one **(b)** or two **(c)** cyclopentane moieties formed by internal cyclization.

**The Supplement related to this article is available online at doi:10.5194/cp-12-1243-2016-supplement.**

**Acknowledgements.** We thank C. Oluseno for fieldwork support, J. Ossebaar for laboratory assistance, A. Hemp for the time series of air temperature near Lake Challa, F. Klein for time series of rainfall reanalysis data, and I. Bessems for data on bulk-sediment composition. The studied sediment sequence was collected with support from the Research Foundation Flanders (FWO-Vlaanderen) and under permit 13/001/11C of the Kenyan Ministry of Education, Science and Technology. The sediment-trap time series was collected with funding from FWO-Vlaanderen and the Netherlands Organization for Scientific Research (NWO) through Euroclimate project CHALLACEA, and diatom analysis was funded by the Federal Science Policy Office of Belgium through the BRAIN-be project PAMEXEA. The organic geochemical analyses producing the principal results presented here received funding from the European Research Council through the European Union's 7th Framework Programme (2007–2013, ERC grant agreement no. 226600). Johan W. H. Weijers acknowledges a Veni grant from NWO. Jaap S. Sinninghe Damsté is supported by the Netherlands Earth System Science Centre (NESSC) though funding from the Ministry of Education, Culture, and Science (OCW).

Edited by: L. Beaufort

## References

Barker, P. A., Hurrell, E. R., Leng, M. J., Wolff, C., Cocquyt, C., Sloane, H. J., and Verschuren, D.: Seasonality in equatorial climate over the last 25 000 years revealed by oxygen isotope records from Mount Kilimanjaro, Geology, 39, 1111–1114, doi:10.1130/G32419.1, 2011.

Barker, P. A., Hurrell, E. R., Leng, M. J., Plessen, B., Wolff, C., Conley, D. J., Keppens, E., Milne, I., Cumming, B. F., Laird, K. R., Kendrick, C. P., Wynn, P. M., and Verschuren D.: Carbon cycling within an East African lake revealed by the carbon isotope composition of diatom silica: a 25 ka record from Lake Challa, Mt. Kilimanjaro, Quaternary Sci. Rev., 66, 55–63, doi:10.1016/j.quascirev.2012.07.016, 2013.

Bessems, I., Verschuren, D., Russell, J. M., Hus, J., Mees, F., and Cumming, B. F.: Palaeolimnological evidence for widespread late 18th century drought across equatorial East Africa, Palaeogeogr. Palaeocl., 259, 107–120, doi:10.1016/j.palaeo.2007.10.002, 2008.

Blaauw, M., van Geel, B., Kristen, I., Plessen, B., Lyaruu, A., Engstrom, D. R., van der Plicht, J., and Verschuren, D.: High-resolution $^{14}$C dating of a 25 000-year lake-sediment record from equatorial East Africa, Quaternary Sci. Rev., 30, 3043–3059, doi:10.1016/j.quascirev.2011.07.014, 2011.

Blaga, C. I., Reichart, G. J., Heiri, O., and Sinninghe Damsté, J. S.: Tetraether membrane lipid distributions in water-column particulate matter and sediments: a study of 47 European lakes along a north-south transect, J. Paleolimnol., 41, 523–540, doi:10.1007/s10933-008-9242-2, 2009.

Brochier-Armanet, C., Boussau, B., Gribaldo, S., and Forterre, P.: Mesophilic Crenarchaeota: proposal for a third archaeal phylum, the Thaumarchaeota, Nat. Rev. Microbiol., 6, 245–252, doi:10.1038/nrmicro1852, 2008.

Buckles, L. K., Villanueva, L., Weijers, J. W. H., Verschuren, D., and Sinninghe Damsté, J. S.: Linking isoprenoidal GDGT membrane-lipid distributions with gene abundances of ammonia-oxidising Thaumarchaeota and uncultured crenarchaeotal groups in the water column of a tropical lake (Lake Challa, East Africa), Environ. Microbiol., 15, 2445–2462, doi:10.1111/1462-2920.12118, 2013.

Buckles, L. K., Weijers, J. W. H., Verschuren, D., and Sinninghe Damsté, J. S.: Sources of core and intact branched tetraether membrane lipids in the lacustrine environment: Anatomy of Lake Challa and its catchment, equatorial East Africa, Geochim. Cosmochim. Ac., 140, 106–126, doi:10.1016/j.gca.2014.04.042, 2014.

Dancey, C. P. and Reidy, J.: Statistics without maths for psychology: Using SPSS for Windows, New York: Prentice Hall, 2004.

Dean, W. E.: Determination of carbonate and organic matter in calcareous sediments and sedimentary rocks by loss on ignition: comparison with other methods, J. Sediment. Petrol., 44, 242–248, 1974.

De Cort, G., Bessems, I., Keppens, E., Mees, F., Cumming, B., and Verschuren, D.: Late-Holocene and recent hydroclimatic variability in the central Kenya Rift Valley: The sediment record of hypersaline lakes Bogoria, Nakuru and Elementeita, Palaeogeogr. Palaeocl., 388, 69–80, doi:10.1016/j.palaeo.2013.07.029, 2013.

DeLong, E. F. and Pace, N. R.: Environmental diversity of Bacteria and Archaea, Syst. Biol., 50, 470–478, doi:10.1080/10635150118513, 2001.

Di, H. J., Cameron, K. C., Shen, J. P., Winefield, C. S., O'Callaghan, M., Bowatte, S., and He, J. Z.: Nitrification driven by bacteria and not archaea in nitrogen-rich grassland soils, Nat. Geosci., 2, 621–624, doi:10.1038/ngeo613, 2009.

Fleitmann, D., Dunbar, R. B., McCulloch, M., Mudelsee, M., Vuille, M., McClanahan, T., Andrews, C., and Mucciarone D. A.: East African soil erosion recorded in a 300-year old coral colony from Kenya, Geophys. Res. Lett., 34, L04401, doi:10.1029/2006GL028525, 2007.

Gasse, F.: Hydrological changes in the African tropics since the Last Glacial Maximum, Quaternary Sci. Rev., 19, 189–211, doi:10.1016/S0277-3791(99)00061-X, 2000.

Hemp, A.: Continuum or zonation? Altitudinal gradients in the forest vegetation of Mt. Kilimanjaro, Plant Ecol., 184, 27–42, doi:10.1007/s11258-005-9049-4, 2006.

Hopmans, E. C., Weijers, J. W. H., Schefuß, E., Herfort, L., Sinninghe Damsté, J. S., and Schouten, S.: A novel proxy for terrestrial organic matter in sediments based on branched and isoprenoid tetraether lipids, Earth Planet. Sc. Lett., 224, 107–116, doi:10.1016/j.epsl.2004.05.012, 2004.

Huguet, C. M., Hopmans, E. C., Febo-Ayala, W., Thompson, D. H., Sinninghe Damsté, J. S., and Schouten, S.: An improved method to determine the absolute abundance of glycerol dibiphytanyl glycerol tetraether lipids, Org. Geochem., 37, 1036–1041, doi:10.1016/j.orggeochem.2006.05.008, 2006.

Inagaki, F., Suzuki, M., Takai, K., Oida, H., Sakamoto, T., Aoki, K., Nealson, K. H., and Horikoshi, K.: Microbial communities

associated with geological horizons in coastal subseafloor sediments from the Sea of Okhotsk, Appl. Environ. Microbiol., 69, 7224–7235, doi:10.1128/AEM.69.12.7224-7235.2003, 2003.

Kaplan, A., Cane, M. A., Kushnir, Y., Clement, A. C., Blumenthal, M. B., and Rajagopalan, B.: Analyses of global sea surface temperature 1856–1991, J. Geophys. Res., 103, 18567–18589, doi:10.1029/97JC01736, 1998.

Kiage, L. M. and Liu, K.-B.: Palynological evidence of climate change and land degradation in the Lake Baringo area, Kenya, East Africa, since AD 1650, Palaeogeogr. Palaeocl., 279, 60–72, doi:10.1016/j.palaeo.2009.05.001, 2009.

Könneke, M., Bernhard, A. E., de la Torre, J. R., Walker, C. B., Waterbury, J. B., and Stahl, D. A.: Isolation of an autotrophic ammonia-oxidizing marine archaeon, Nature, 437, 543–546, doi:10.1038/nature03911, 2005..

Leininger, S., Urich, T., Schloter, M., Schwark, L., Qi, J., Nicol, G. W., Prosser, J. I., Schuster, S. C., and Schleper, C.: Archaea predominate among ammonia-oxidizing prokaryotes in soils, Nature, 442, 806–809, doi:10.1038/nature04983, 2006.

Lengger, S. K., Hopmans, E. C., Sinninghe Damsté, J. S., and Schouten, S.: Comparison of extraction and work up techniques for analysis of core and intact polar tetraether lipids from sedimentary environments, Org. Geochem., 47, 34–40, doi:10.1016/j.orggeochem.2012.02.009, 2012.

Lipp, J. S. and Hinrichs, K.: Structural diversity and fate of intact polar lipids in marine sediments, Geochim. Cosmochim. Ac., 73, 6816–6833, doi:10.1016/j.gca.2009.08.003, 2009.

Loomis, S. E., Russell, J. M., and Sinninghe Damsté, J. S.: Distributions of branched GDGTs in soils and lake sediments from western Uganda: Implications for a lacustrine paleothermometer, Org. Geochem., 42, 739–751, doi:10.1016/j.orggeochem.2011.06.004, 2011.

Mann, M. E., Cane, M. A., Zebiak, S. E., and Clement, A.: Volcanic and solar forcing of the tropical Pacific over the past 1000 years, J. Clim., 18, 447–456, doi:10.1175/JCLI-3276.1, 2005.

Martens-Habbena, W., Berube, P. M., Urakawa, H., de la Torre, J. R., and Stahl, D. A.: Ammonia oxidation kinetics determine niche separation of nitrifying Archaea and Bacteria, Nature, 461, 976–979, doi:10.1038/nature08465, 2009.

Moernaut, J., Verschuren, D., Charlet, F., Kristen, I., Fagot, M., and De Batist, M.: The seismic-stratigraphic record of lake-level fluctuations in Lake Challa: hydrological stability and change in equatorial East-Africa over the last 140 kyr, Earth Planet. Sc. Lett., 290, 214–223, doi:10.1016/j.epsl.2009.12.023, 2010.

Nicholson, S. E. and Yin, X.: Rainfall conditions in equatorial East Africa during the nineteenth century as inferred from the record of Lake Victoria, Climatic Change, 48, 387–398, doi:10.1023/A:1010736008362, 2001.

Nicholson, S. E., Klotter, D., and Dezfuli, A. K.: Spatial reconstruction of semi-quantitative precipitation fields over Africa during the nineteenth century from documentary evidence and gauge data, Quaternary Res., 78, 13–23, doi:10.1016/j.yqres.2012.03.012, 2012.

Oppermann, B. I., Michaelis, W., Blumenberg, M., Frerichs, J., Schulz, H. M., Schippers, A., Beaubien, S. E., and Krüger, M.: Soil microbial community changes as a result of long-term exposure to a natural $CO_2$ vent, Geochim. Cosmochim. Ac., 74, 2697–2716, doi:10.1016/j.gca.2010.02.006, 2010.

Payne, B. R.: Water balance of Lake Chala and its relation to groundwater from tritium and stable isotope data, J. Hydrol., 11, 47–58, doi:10.1016/0022-1694(70)90114-9, 1970.

Pitcher, A., Hopmans, E. C., Mosier, A. C., Park, S., Rhee, S., Francis, C. A., Schouten, S., and Sinninghe Damsté, J. S.: Core and intact polar glycerol dibiphytanyl glycerol tetraether lipids of ammonia-oxidizing archaea enriched from marine and estuarine sediments, Appl. Environ. Microbiol. 77, 3468–3477, doi:10.1128/AEM.02758-10, 2011a.

Pitcher, A., Villanueva L., Hopmans E. C., Schouten S., Reichart G.-J., and Sinninghe Damsté J. S.: Niche segregation of ammonia-oxidizing archaea and annamox bacteria in the Arabian Sea oxygen minimum zone, ISME J., 5, 1896–1904, doi:10.1038/ismej.2011.60, 2011b.

Pitcher, A., Wuchter, C., Siedenberg, K., Schouten, S., and Sinninghe Damsté, J. S.: Crenarchaeol tracks winter blooms of planktonic, ammonia-oxidizing Thaumarchaeota in the coastal North Sea, Limnol. Oceanogr., 56, 2308–2318, doi:10.4319/lo.2011.56.6.2308, 2011c.

Rayner, N. A., Parker, D. E., Horton, E. B., Folland, C. K., Alexander, L. V., Rowell, D. P., Kent, E. C., and Kaplan, A.: Global analyses of sea surface temperature, sea ice, and night marine air temperature since the late nineteenth century, J. Geophys. Res. Atmos. 108, 4407, doi:10.1029/2002JD002670, 2003.

Ropelewski, C. F. and Jones, P. D.: An extension of the Tahiti-Darwin southern oscillation index, Mon. Weath. Rev., 115, 2161–2165, 1987.

Russell, J. M. and Johnson, T. C.: A high resolution geochemical record from Lake Edward, Uganda-Congo, and the timing and causes of tropical African drought during the late Holocene, Quaternary Sci. Rev., 24, 1375–1389, doi:10.1016/j.quascirev.2004.10.003, 2005.

Russell, J. M. and Johnson, T. C.: Little Ice Age drought in equatorial Africa: Intertropical Convergence Zone migrations and El Niño-Southern Oscillation variability, Geology, 35, 21–24, doi:10.1130/G23125A.1, 2007.

Russell, J. M., Verschuren, D., and Eggermont, H.: Spatial complexity of "Little Ice Age" climate in East Africa: sedimentary records from two crater lake basins in western Uganda, Holocene, 17, 183–193, doi:10.1177/0959683607075832, 2007.

Schneider, U., Becker, A., Finger, P., Meyer-Christoffer, A., Ziese, M., and Rudolf, B.: GPCC's new land surface precipitation climatology based on quality-controlled in situ data and its role in quantifying the global water cycle, Theor. Appl. Climatol., 115, 15–40, doi:10.1007/s00704-013-0860-x, 2014.

Schouten, S., Hopmans, E. C., Schefuss, E., and Sinninghe Damsté, J. S.: Distributional variations in marine crenarchaeotal membrane lipids: a new tool for reconstructing ancient sea water temperatures?, Earth Planet. Sc. Lett., 204, 265–274, doi:10.1016/S0012-821X(02)00979-2, 2002.

Schouten, S., Huguet, C., Hopmans, E. C., Kienhuis, M. V. M., and Sinninghe Damsté, J. S.: Analytical methodology for $TEX_{86}$ paleothermometry by high-performance liquid chromatography/atmospheric pressure chemical ionization-mass spectrometry, Anal. Chem., 79, 2940–2944, doi:10.1021/ac062339v, 2007.

Schouten, S., Hopmans, E. C., and Sinninghe Damsté, J. S.: The organic geochemistry of glycerol dialkyl glycerol tetraether lipids: A review, Org. Geochem., 54, 19–61, doi:10.1016/j.orggeochem.2012.09.006, 2013.

Schubotz, F., Wakeham, S. G., Lipp, J. S., Fredricks, H. F., and Hinrichs, K.: Detection of microbial biomass by intact polar membrane lipid analysis in the water column and surface sediments of the Black Sea, Environ. Microbiol., 11, 2720–2734, doi:10.1111/j.1462-2920.2009.01999.x, 2009.

Sinninghe Damsté, J. S., Schouten, S., Hopmans, E. C., van Duin, A. C. T., and Geenevasen, J. A. J.: Crenarchaeol: the characteristic core glycerol dibiphytanyl glycerol tetraether membrane lipid of cosmopolitan pelagic crenarchaeota, J. Lipid Res., 43, 1641–1651, doi:10.1194/jlr.M200148-JLR200, 2002.

Sinninghe Damsté, J. S., Ossebaar, J., Abbas, B., Schouten, S., and Verschuren, D.: Fluxes and distribution of tetraether lipids in an equatorial African lake: Constraints on the application of the $TEX_{86}$ palaeothermometer and BIT index in lacustrine settings, Geochim. Cosmochim. Ac., 73, 4232–4249, doi:10.1016/j.gca.2009.04.022, 2009.

Sinninghe Damsté, J. S., Rijpstra, W. I. C., Hopmans, E. C., Weijers, J. W. H., Foesel, B. U., Overmann, J., and Dedysh, S. N.: 13,16-Dimethyl octacosanedioic acid (iso-diabolic acid), a common membrane-spanning lipid of acidobacteria subdivisions 1 and 3, Appl. Environ. Microbiol., 77, 4147–4154, doi:10.1128/AEM.00466-11, 2011.

Sinninghe Damsté, J. S., Ossebaar, J., Schouten, S., and Verschuren, D.: Distribution of tetraether lipids in the 25-ka sedimentary record of Lake Challa: extracting reliable $TEX_{86}$ and MBT/CBT palaeotemperatures from an equatorial African lake, Quaternary Sci. Rev., 50, 43–54, doi:10.1016/j.quascirev.2012.07.001, 2012a.

Sinninghe Damsté, J. S., Rijpstra, W. I. C., Hopmans, E. C., Man-Young, J., Kim, J.-K., Rhee, S.-K., Stieglmeier, M., and Schleper, C.: Intact polar and core glycerol dibiphytanyl glycerol tetraether lipids of Group 1.1a and 1.1b Thaumarchaeota in soil, Appl. Environ. Microbiol., 78, 6866–6874, doi:10.1128/AEM.01681-12, 2012b.

Sinninghe Damsté, J. S., Rijpstra, W. I. C., Hopmans, E. C., Foesel, B., Wüst, P., Overmann, J., Tank, M., Bryant, D., Dunfield, P., Houghton, K., and Stott, M.: Ether- and ester-bound iso-diabolic acid and other lipids in Acidobacteria of subdivision 4, Appl. Environ. Microbiol., 80, 5207–5218, doi:10.1128/AEM.01066-14, 2014.

Spang, A., Hatzenpichler, R., Brochier-Armanet, C., Rattei, T., Tischler, P., Spieck, E., Streit, W., Stahl, D. A., Wagner, M., and Schleper, C.: Distinct gene set in two different lineages of ammonia-oxidizing archaea supports the phylum Thaumarchaeota, Trends Microbiol., 18, 331–340, doi:10.1016/j.tim.2010.06.003, 2010.

Stager, J. C., Ryves, D., Cumming, B. F., Meeker, L. D., and Beer, J.: Solar variability and the levels of Lake Victoria, East Africa, during the last millennium, J. Paleolimnol., 33, 243–251, doi:10.1007/s10933-004-4227-2, 2005.

Tierney, J. E. and Russell, J. M.: Distributions of branched GDGTs in a tropical lake system: Implications for lacustrine application of the MBT/CBT paleoproxy, Org. Geochem., 40, 1032–1036, doi:10.1016/j.orggeochem.2009.04.014, 2009.

Tierney, J. E., Russell, J. M., Eggermont, H., Hopmans, E. C., Verschuren, D., and Sinninghe Damsté, J. S.: Environmental controls on branched tetraether lipid distributions in tropical East African lake sediments, Geochim. Cosmochim. Ac., 74, 4902–4918, doi:10.1016/j.gca.2010.06.002, 2010.

Tierney, J. E., Smerdon, J. E., Anchukaitis, K. J., and Seager, R.: Multidecadal variability in East African hydroclimate controlled by the Indian Ocean, Nature, 493, 389–392, doi:10.1038/nature11785, 2013.

Uthermöhl, H.: Neue Wege in der quantitativen Erfassung des Planktons, Verh. Int. Ver. Theor. Angew. Limnol., 5, 567–596, 1931.

Verschuren, D.: Influence of depth and mixing regime on sedimentation in a small, fluctuating tropical soda lake, Limnol. Oceanogr., 44, 1103–1113, doi:10.4319/lo.1999.44.4.1103, 1999.

Verschuren, D.: Reconstructing fluctuations of a shallow East African lake during the past 1800 yrs from sediment stratigraphy in a submerged crater basin, J. Paleolimnol., 25, 297–311, doi:10.1023/A:1011150300252, 2001.

Verschuren, D.: Decadal and century-scale climate variability in tropical Africa during the past 2000 years, in: Past Climate Variability through Europe and Africa, edited by: Battarbee, R., Gasse, F., and Stickley, C., Springer, Netherlands, 139–158, doi:10.1007/978-1-4020-2121-3_8, 2004.

Verschuren, D. and Charman, D.: Latitudinal linkages in late-Holocene moisture-balance variation, in: Natural Climate Variability and Global Warming, edited by: Battarbee, R. W. and Binney, H. A., Wiley-Blackwell, Chichester, 189–231, doi:10.1002/9781444300932.ch8, 2000.

Verschuren, D., Tibby, J., Leavitt, P. R., and Roberts, C. N.: The environmental history of a climate-sensitive lake in the former "White Highlands" of central Kenya, Ambio, 28, 494–501, 1999.

Verschuren, D., Laird, K. R., and Cumming, B. F.: Rainfall and drought in equatorial east Africa during the past 1100 years, Nature, 403, 410–414, doi:10.1038/35000179, 2000.

Verschuren, D., Sinninghe Damsté, J. S., Moernaut, J., Kristen, I., Blaauw, M., Fagot, M., Haug, G. H., and CHALLACEA project members: Half-precessional dynamics of monsoon rainfall near the East African Equator, Nature, 462, 637–641, doi:10.1038/nature08520, 2009.

Wang, H., Liu, W., Zhang, C. L., Liu, Z., and He, Y.: Branched and isoprenoid tetraether (BIT) index traces water content along two marsh-soil transects surrounding Lake Qinghai: Implications for paleo-humidity variation, Org. Geochem. 59, 75–81, doi:10.1016/j.orggeochem.2013.03.011, 2013.

Weltje, G. J. and Tjallingii, R.: Calibration of XRF core scanners for quantitative geochemical logging of soft sediment cores: theory and application, Earth Planet. Sc. Lett., 274, 423–438, doi:10.1016/j.epsl.2008.07.054, 2008.

Weijers, J. W. H., Schouten, S., van der Linden, M., van Geel, B., and Sinninghe Damsté, J. S.: Water table related variations in the abundance of intact archaeal membrane lipids in a Swedish peat bog, FEMS Microbiol. Lett., 239, 51–56, doi:10.1016/j.femsle.2004.08.012, 2004.

Weijers, J. W. H., Schouten, S., Hopmans, E. C., Geenevasen, J. A. J., David, O. R. P., Coleman, J. M., Pancost, R. D., and Sinninghe Damsté, J. S.: Membrane lipids of mesophilic anaerobic bacteria thriving in peats have typical archaeal traits, Environ. Microbiol., 8, 648–657, doi:10.1111/j.1462-2920.2005.00941.x, 2006.

Weijers, J. W. H., Schouten, S., van den Donker, J. C., Hopmans, E. C., and Sinninghe Damsté, J. S.: Environmental controls on bacterial tetraether membrane lipid distribution in soils, Geochim.

Cosmochim. Ac., 71, 703–713, doi:10.1016/j.gca.2006.10.003, 2007.

Weijers, J. W. H., Panoto, E., van Bleijswijk, J., Schouten, S., Rijpstra, W. I. C., Balk, M., Stams, A. J. M., and Sinninghe Damsté, J. S.: Constraints on the biological source(s) of the orphan branched tetraether membrane lipids, Geomicrobiol. J., 26, 402–414, doi:10.1080/01490450902937293, 2009a.

Weijers, J. W. H., Schouten, S., Schefuss, E., Schneider, R. R., and Sinninghe Damsté, J. S.: Disentangling marine, soil and plant organic carbon contributions to continental margin sediments: A multi-proxy approach in a 20 000 year sediment record from the Congo deep-sea fan, Geochim. Cosmochim. Ac., 73, 119–132, doi:10.1016/j.gca.2008.10.016, 2009b.

Weijers, J. W. H., Wiesenberg, G. L. B., Bol, R., Hopmans, E. C., and Pancost, R. D.: Carbon isotopic composition of branched tetraether membrane lipids in soils suggest a rapid turnover and a heterotrophic life style of their source organism(s), Biogeosciences, 7, 2959–2973, doi:10.5194/bg-7-2959-2010, 2010.

Wolff, C.: East African monsoon variability since the last glacial, PhD Thesis, Universität Potsdam, 2012.

Wolff, C., Haug, G. H., Timmermann, A., Sinninghe Damsté, J. S., Brauer, A., Sigman, D. M., Cane, M. A., and Verschuren, D.: Reduced interannual rainfall variability in East Africa during the Last Ice Age, Science, 333, 743–747, doi:10.1126/science.1203724, 2011.

Wolff, C., Kristen-Jenny, I., Schettler, G., Plessen, B., Meyer, H., Dulski, P., Naumann, R., Brauer, A., Verschuren, D., and Haug, G. H.: Modern seasonality in Lake Challa (Kenya/Tanzania) and its sedimentary documentation in recent lake sediments, Limnol. Oceanogr., 59, 621–1636, doi:10.4319/lo.2014.59.5.1621, 2014.

Wuchter, C., Schouten, S., Coolen, M.J . L., and Sinninghe Damsté, J. S.: Temperature-dependent variation in the distribution of tetraether membrane lipids of marine Crenarchaeota: Implications for $TEX_{86}$ paleothermometry, Paleoceanography, 19, PA4028, doi:10.1029/2004PA001041, 2004.

Wuchter, C., Abbas, B., Coolen, M. J. L., Herfort, L., van Bleijswijk, J., Timmers, P., Strous, M., Teira, E., Herndl G. J., Middelburg, J. J., Schouten, S., and Sinninghe Damsté, J. S.: Archaeal nitrification in the ocean, P. Natl. Acad. Sci USA, 103, 12317–12322, doi:10.1073/pnas.0600756103, 2006.